Heliyon

Received:
11 August 2015
Revised:
4 November 2015
Accepted:
5 November 2015

Heliyon (2015) e00046

Mesendogen, a novel inhibitor of TRPM6, promotes mesoderm and definitive endoderm differentiation of human embryonic stem cells through alteration of magnesium homeostasis

Yijie Geng *, **Bradley Feng**

Department of Cell and Developmental Biology, University of Illinois at Urbana–Champaign, Urbana, IL 61801, USA

* Corresponding author. Tel.: +217 390 3210.

E-mail address: geng2@illinois.edu (Y. Geng).

Abstract

The homo- and hetero-tetrameric channel complexes formed by transient receptor potential cation channel, subfamily M, member 6 (TRPM6) and 7 (TRPM7) (collectively referred to as TRPM6/TRPM7 channels in this study) are the major regulators of cellular magnesium uptake, yet the exact roles of TRPM6/TRPM7 channels and cellular magnesium homeostasis during development are poorly understood. Here, we report a novel small molecule Mesendogen (MEG) which robustly induces nearly homogeneous (≥85%) mesoderm and definitive endoderm (DE) differentiations of human embryonic stem cells (hESCs) in combination with growth factors. A kinome screen followed by loss-of-function experiments identified TRPM6 as the biological target of MEG. We demonstrated that MEG functions by inhibiting TRPM6/TRPM7 magnesium channel activity, as MEG reduced intracellular magnesium level, while TRPM6/TRPM7 channel modulation and magnesium-withdrawal

http://dx.doi.org/10.1016/j.heliyon.2015.e00046

phenocopied MEG at enhancing mesoderm and DE differentiations. This study discovers a robust chemical enhancer of hESC directed differentiation, and uncovers a novel regulatory role of cellular magnesium homeostasis during early embryonic cell fate specification.

Keywords: Biological sciences, Early embryonic development, Stem cells, Cell differentiation

1. Introduction

Transient receptor potential cation channel, subfamily M, member 6 (TRPM6) and 7 (TRPM7) are known as "channel kinases" in that they contain both an intracellular kinase domain and a transmembrane channel domain (Chubanov et al., 2005a; Chubanov et al., 2007; Chubanov et al., 2006; Chubanov et al., 2005b; Chubanov et al., 2004; Schlingmann et al., 2007). The homo- and hetero-tetrameric channel complexes formed by TRPM6 and TRPM7 are believed to be the major ion channels responsible for cellular magnesium import (Chubanov et al., 2005b; Chubanov et al., 2004; Schlingmann et al., 2007).

Although the role of Mg^{2+} in maintaining normal physiological functions of various adult organs and tissues has been well-established, its function during early embryonic development remains poorly understood. Mg^{2+} deficiency has been shown to cause severe developmental defects in *Xenopus laevis* and rats (Hurley et al., 1976; Miller and Landesman, 1977; Wang et al., 1971), and has been linked to birth defects in humans, in particular to the neural tube closure defect spina bifida (Groenen et al., 2004). Results from loss-of-function studies of TRPM6/TRPM7 channel corroborate with these findings, as mice defective inTRPM6 displayed embryonic mortality and neural tube defects (Walder et al., 2009), while TRPM7-knockout mice died before day 7.5 of embryogenesis (E7.5) (Jin et al., 2008; Jin et al., 2012). In *Xenopus laevis*, TRPM7 depletion by morpholino resulted in neural tube closure defect and dorsal-flexure, with the development of anterior structures of the embryo severely reduced or missing; this phenotype was partially rescued by Mg^{2+} supplementation or forced expression of TRPM6 (Liu et al., 2011). The dysregulation of noncanonical Wnt pathway or planar cell polarity (PCP) pathway, the pathway regulating convergent extension movement during gastrulation, has been proposed as the underlying cause of the neural tube closure defect phenotype observed in *Xenopus laevis* (Liu et al., 2011), although not without debate (Komiya et al., 2014; Walder et al., 2009) (Discussion). These observations suggest a potentially key regulatory role of Mg^{2+} during early embryonic development, toward which controversy remains and a thorough understanding has not been acquired.

In this study, through a small scale chemical screen, we discovered a novel small molecule Mesendogen (MEG for short) that robustly enhanced the growth

http://dx.doi.org/10.1016/j.heliyon.2015.e00046

factor-induced mesoderm and DE differentiations of human embryonic stem cells (hESCs) and human induced pluripotent stem cells (hiPSCs) to near-homogeneity (≥85%). Using target identification techniques followed by functional validations, we identified TRPM6 as the biological target of MEG. We further demonstrated that MEG treatment in hESCs effectively reduced cellular magnesium level, and that inhibition of the magnesium-importing activity of TRPM6/TRPM7 channel complexes by known channel modulators and withdrawal of Mg^{2+} in differentiation medium gave rise to similar differentiation-enhancing phenotypes as compared to MEG. These data suggest that MEG exerts its biological function by acting as an inhibitor of TRPM6/TRPM7 channels and, subsequently, by modulating cellular Mg^{2+} uptake. This study for the first time uncovers a regulatory role of Mg^{2+} in embryonic cell fate determination, in addition to its previously proposed role in regulating cell movement during gastrulation (Liu et al., 2011).

2. Results

2.1. Small scale chemical screening identified a novel small molecule that induces mesoderm and endoderm, but not neural differentiation of human embryonic stem cells (hESCs)

We previously conducted a high-throughput chemical screening and found 29 bioactive small molecules that potently disrupt hESC pluripotency (Geng et al., 2015). Using this compound collection we conducted a small scale chemical screen (Materials and Methods) to search for small molecules that specifically induce mesoderm and DE differentiations, and identified compound 6528694 (N-({[2-chloro-5-(trifluoromethyl) phenyl]amino}carbonothioyl)-4-isopropylbenzamide; Fig. 1A). The colony integrity of hESCs was lost after treated with 6528694 at 10 μM for 4 days, as evidenced by cells within the colonies spread out and migrated away from each other (Fig. 1B). A 7-day treatment of 6528694 in hESCs maintained under a pluripotency culture condition ("mTeSR1" condition hereafter) (Ludwig et al., 2006) induced elevated protein expressions of mesoderm markers T (Brachuary) and EOMES (Eomesodermin) and DE markers SOX17 and FOXA2, but not neural-specific markers PAX6 and SOX1 (Fig. 1B). Meanwhile pluripotency was disrupted as expected, shown by downregulations of the pluripotency markers OCT4 and SOX2 (also a neural differentiation marker) (Fig. 1C). We thus name this compound Mesendogen, short for Mesoderm and Definitive Endoderm Inducing Reagent, and hereafter refer to this molecule as MEG for short.

The sole fact that lineage-specific markers were elevated upon MEG treatment cannot prove that mesoderm or DE progenitors have been successfully generated. To prove the existence of such a population, one must demonstrate

http://dx.doi.org/10.1016/j.heliyon.2015.e00046

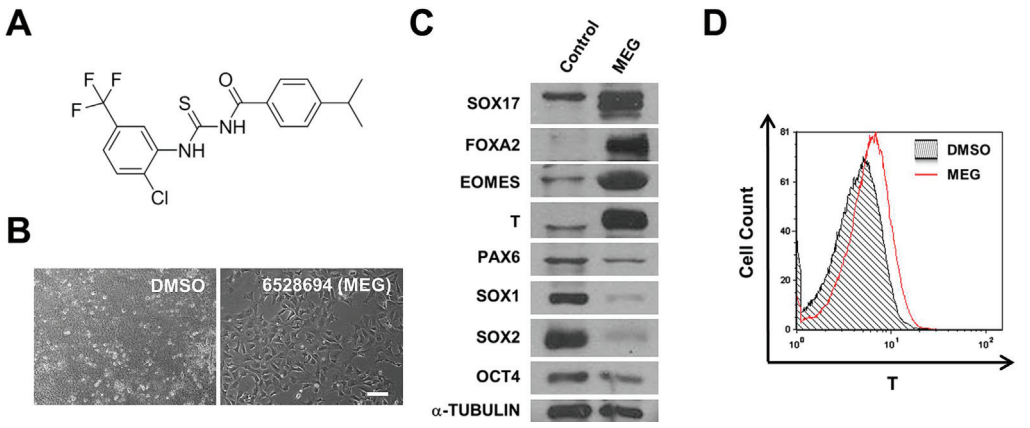

Fig. 1. Compound 6528694 (Mesendogen) induces hESC mesoderm and endoderm differentiation. (A) Chemical structure of compound 6528694 (Mesendogen or MEG). (B) Phase contrast images of H1 hESCs treated with DMSO and 6528694 (MEG, 10 μM) for 4 days in mTeSR1 medium. Scale bar: 100 μm. (C) Western blotting of endoderm markers SOX17 and FOXA2, mesoderm markers T and EOMES, neural-specific markers SOX1 and PAX6, and pluripotency markers OCT4 and SOX2 in undifferentiated H9 hESCs (Control) or H9 hESCs treated with 6528694 (MEG, 10 μM) for 7 days while maintained in mTeSR1 medium. α-TUBULIN was used as a loading control. (D) FACS analysis of T in H9 hESCs treated with DMSO and MEG (5 μM) for 4 days. $n = 4$ independent experiments.

the emergence of a distinct cell population that expresses progenitor markers at the single cell level. However, MEG treatment alone was insufficient to induce such a distinct mesoderm progenitor population: when incubated with hESCs in a growth factor-free mesoderm basal differentiation medium (Materials and Methods), MEG marginally increased T expression in the overall population, but failed to drive the differentiation of a distinct T^+ population compared to the DMSO control, as shown by FACS analysis (Fig. 1D). We therefore decided to test whether MEG could enhance the efficiencies of growth factor-guided mesoderm and DE differentiation protocols at generating mesoderm and DE progenitors.

2.2. MEG induces nearly homogeneous mesoderm differentiation in combination with growth factors

To test the effect of MEG in growth factor-induced mesoderm differentiation, we first derived a 2-dimensional (2-D) growth factor-guided mesoderm induction protocol (Fig. 2A and Materials and Methods; "A-BVF" method hereafter) modified based on previous publications (Bernardo et al., 2011; Evseenko et al., 2010; Yu et al., 2011). Briefly, Activin A (A), bone morphogenetic protein 4 (BMP4; B), vascular endothelial growth factor (VEGF; V), and basic fibroblast growth factor (bFGF; F) were used to drive differentiation; cells were analyzed after 1.5–2 days of induction (Fig. 2A and Materials and Methods). Using this method, we found that mesoderm differentiation efficiencies highly depended on

http://dx.doi.org/10.1016/j.heliyon.2015.e00046

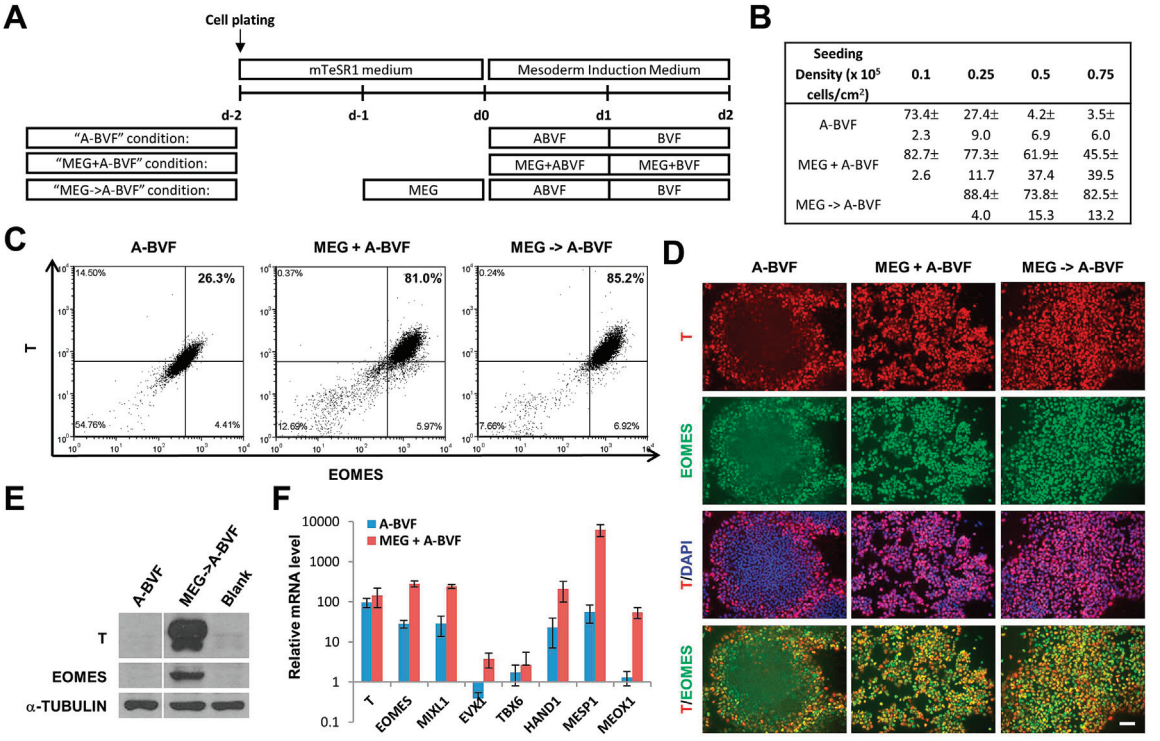

Seeding Density (x 10^5 cells/cm^2)	0.1	0.25	0.5	0.75
A-BVF	73.4± 2.3	27.4± 9.0	4.2± 6.9	3.5± 6.0
MEG + A-BVF	82.7± 2.6	77.3± 11.7	61.9± 37.4	45.5± 39.5
MEG -> A-BVF		88.4± 4.0	73.8± 15.3	82.5± 13.2

Fig. 2. MEG induces nearly homogeneous mesoderm differentiation in combination with the A-BVF condition. (A) Schematic overviews of mesoderm differentiation conditions used in this study. (B) Summary of FACS results showing the percentages of T^+EOMES^+ population acquired after 2 days of mesoderm differentiation of H9 and H1 hESCs under various plating densities and differentiation conditions. Results from six independent experiments ($n = 6$) are shown as mean ± SD; 3–4 data points were collected and analyzed for each condition. (C) FACS analysis of T and EOMES in H9 hESCs treated with mesoderm differentiation conditions including A-BVF, MEG+A-BVF, and MEG->A-BVF. Cells were plated at 0.25 × 10^5 cells/cm^2. (D) Immunofluorescent staining of T (red) and EOMES (green) in H1 hESCs induced to undergo mesoderm differentiation for ~1.5 days under various conditions. Nuclei were stained with DAPI (blue). Cells were plated at 0.25 × 10^5 cells/cm^2 for A-BVF condition, 0.75 × 10^5 cells/cm^2 for MEG+A-BVF condition, and 1.0 × 10^5 cells/cm^2 for MEG->A-BVF condition. (E) Western blotting of T and EOMES in H9 hESCs induced to undergo mesoderm differentiation for 2 days under A-BVF and MEG->A-BVF conditions. Cells cultured in mesoderm basal medium without growth factors were used as a control (Blank). Cells were plated at 1.0 × 10^5 cells/cm^2. α-TUBULIN was used as a loading control. (F) Quantitative-PCR analysis of mesoderm markers in H9 hESCs under A-BVF and MEG+A-BVF conditions for 2 days. All values were normalized to the mRNA level (=1) in cells cultured in mesoderm basal medium without growth factors. Each bar represents the mean ± SD (error bars). $n = 2$ independent experiments. ACTB (β-actin) was used as a loading control.

the initial plating densities of hESCs: the lowest plating density tested (0.1 × 10^5 cells/cm^2) gave the highest yield of T^+EOMES^+ cells (73.4 ± 2.3% by FACS; Fig. 2B) which represent mesoderm progenitors; this efficiency quickly dropped to <5% at and above 0.5 × 10^5 cells/cm^2 (Fig. 2B).

We then added MEG to the A-BVF induction protocol, either by directly combining with the growth factors (Fig. 2A; "MEG+A-BVF" or "combination"

http://dx.doi.org/10.1016/j.heliyon.2015.e00046

condition hereafter) or by pre-incubating in mTeSR1 medium for 24 hours before starting the growth factor treatments (Fig. 2A; "MEG->A-BVF" or "pre-treatment" condition hereafter). Both approaches dramatically improved the induction efficiencies of A-BVF in all plating densities tested (Fig. 2B). Most notably, the combination condition enhanced the differentiation efficiency (measured by percentage of $T^+/EOMES^+$ cells) at the density of 0.1×10^5 cells/cm^2 from 73.4 ± 2.3% for the A-BVF condition to an average of 82.7 ± 2.6%, whereas the pre-treatment condition dramatically enhanced the efficiency at 0.25×10^5 cells/cm^2 from 27.4 ± 9.0% to 88.4 ± 4.0% (Fig. 2B). An example of nearly homogeneous mesoderm differentiation at 0.25×10^5 cells/cm^2 plating density under both the pre-treatment condition and the combination condition is shown in Fig. 2C. Similar results were acquired through immunofluorescence staining (Fig. 2D) and Western blotting (Fig. 2E) using the same markers T and EOMES, and through qPCR using a range of mesoderm markers including *T*, *EOMES*, *MIXL1*, *EVX1*, *TBX6*, *HAND1*, *MESP1*, and *MEOX1* (Fig. 2F).

We find one technical question particularly worth noting for the FACS analyses which is that undifferentiated hESCs already possess significant background signals for T and EOMES. If isotype controls were used to set up quadrants for the dot plots, these background signals will lead to an extremely high false positive rate for the detection of T^+EOMES^+ population (98.42% T^+EOMES^+; Fig. 3A). Thus, undifferentiated hESCs stained for T and EOMES, instead of isotype IgG controls, were used as gating controls for mesoderm-differentiation FACS analyses performed in this study (unless otherwise specified) to ensure a stringent quantification of the differentiation efficiencies (Materials and Methods).

The mesoderm differentiation-enhancing effect of MEG is robust and is not limited to hESCs or to the A-BVF differentiation condition. MEG effectively enhanced the mesoderm differentiation efficiency of a human induced pluripotent stem cell (hiPSC) line MMW2 (Mali et al., 2010) in a similar fashion as compared to its effect in hESCs (Fig. 3B). MEG also improved the efficiencies of variations of mesoderm induction conditions adopted from reported methods with modifications, such as BVF condition (Bernardo et al., 2011) (BMP4, VEGF, and bFGF; Fig. 3C) and BF condition (Bernardo et al., 2011; Yu et al., 2011) (BMP4 and bFGF; Fig. 3D). Detailed protocols for these conditions are described in Materials and Methods.

2.3. MEG induces nearly homogeneous definitive endoderm differentiation in combination with growth factors

To test whether MEG enhances growth factor-induced DE differentiation in a similar fashion as compared to its effects in mesoderm differentiation, we first established a 2-D growth factor-guided DE induction protocol (Fig. 4A and

http://dx.doi.org/10.1016/j.heliyon.2015.e00046

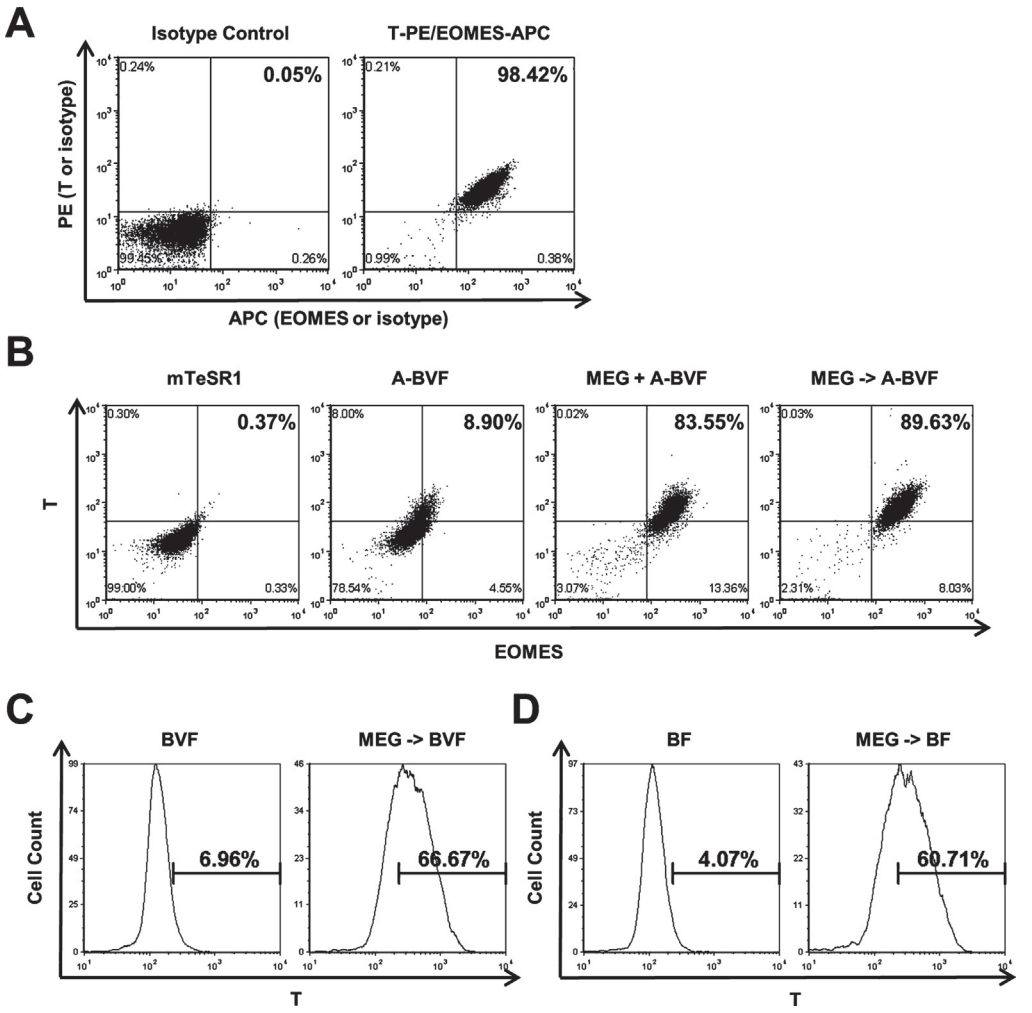

Fig. 3. MEG enhances mesoderm differentiation of hiPSCs and of variations of mesoderm induction conditions. (A) FACS analysis of PE and APC in H9 hESCs cultured in mTeSR1 medium. Cells were stained with T-PE and EOMES-APC antibodies (T-PE/EOMES-APC) or non-specific IgG isotype control antibodies conjugated with the same fluorophores (isotype control). Isotype IgG, when used as a gating control, gave rise to a high percentage of false-positive cells in the undifferentiated mTeSR1 culture (98.42% $PE^{+}APC^{+}$ in the T-PE/EOMES-APC stained sample). $n > 10$ independent experiments. (B) FACS analysis of T and EOMES in MMW2 hiPSCs differentiated in A-BVF, MEG+A-BVF, and MEG->A-BVF conditions for 2 days. Cells were plated at 0.5×10^5 cells/cm^2 for A-BVF and MEG->A-BVF conditions and 0.25×10^5 cells/cm^2 for MEG+A-BVF condition. Cells cultured in mTeSR1 medium were used as a gating control. $n = 2$ independent experiments. (C) FACS analysis of T in H1 hESCs differentiated in BMP4 (10 ng/ml), VEGF (10 ng/ml), and bFGF (20 ng/ml) (BVF condition) for 1.5 days, with or without MEG (10 μM) pre-treatment. $n = 2$ independent experiments. (D) FACS analysis of T in H1 hESCs differentiated in BMP4 (10 ng/ml) and bFGF (20 ng/ml) (BF condition) for 1.5 days, with or without MEG pre-treatment. $n > 5$ independent experiments.

http://dx.doi.org/10.1016/j.heliyon.2015.e00046

Materials and Methods; "AWS" method hereafter) designed based on reported methods (Borowiak et al., 2009; D'Amour et al., 2005) with modifications. Briefly, Activin A (A), WNT3A (W), and increasing concentrations of fetal bovine serum (S) were applied to drive differentiation; cells were analyzed after 5–7 days of induction (Fig. 4A and Materials and Methods). DE differentiation efficiencies were measured by FACS analyses by quantifying the percentage of

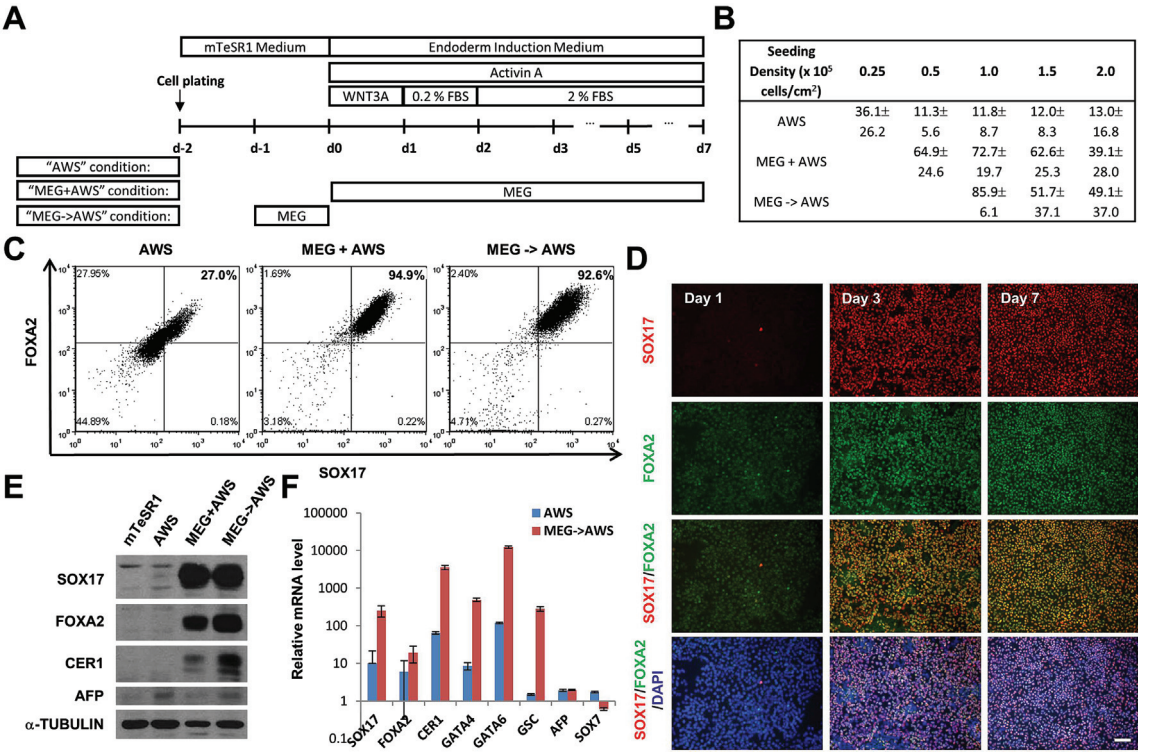

Seeding Density (x 10^5 cells/cm^2)	0.25	0.5	1.0	1.5	2.0
AWS	36.1± 26.2	11.3± 5.6	11.8± 8.7	12.0± 8.3	13.0± 16.8
MEG + AWS		64.9± 24.6	72.7± 19.7	62.6± 25.3	39.1± 28.0
MEG -> AWS			85.9± 6.1	51.7± 37.1	49.1± 37.0

Fig. 4. MEG induces nearly homogeneous definitive endoderm differentiation in combination with the AWS condition. (A) Schematic overviews of definitive endoderm differentiation conditions used in this study. (B) Summary of FACS results showing the percentages of $SOX17^+FOXA2^+$ population acquired after 7 days of definitive endoderm differentiation of H1 and H9 hESCs under various plating densities and differentiation conditions. Results from six independent experiments ($n = 6$) are shown as mean ± SD; 3–5 data points were collected and analyzed for each condition. (C) FACS analysis of SOX17 and FOXA2 in H1 hESCs treated with definitive endoderm differentiation conditions including AWS, MEG+AWS, and MEG->AWS for 7 days. Cells were plated at 1.0×10^5 cells/cm^2. (D) Immunofluorescent staining of SOX17 (red) and FOXA2 (green) in H9 hESCs induced to undergo definitive endoderm differentiation under the MEG->AWS condition for 1, 3, and 7 days. Nuclei were stained with DAPI (blue). Scale bar: 100 μm. (E) Western blotting of SOX17, FOXA2, CER1, and AFP in H9 hESCs induced to undergo definitive endoderm differentiation under AWS, MEG+AWS, and MEG->AWS conditions for 7 days. Cells cultured in mTeSR1 medium were used as a control (mTeSR1). Cells were plated at 0.25×10^5 cells/cm^2 for the AWS condition, 1.0×10^5 cells/cm^2 for the MEG+AWS condition, and 1.5×10^5 cells/cm^2 for the MEG->AWS condition. α-TUBULIN was used as a loading control. (F) Quantitative-PCR analysis of endoderm markers in H9 hESCs under AWS and MEG->AWS conditions for 5 days. All values were normalized to the mRNA level (=1) in cells cultured in mTeSR1 medium. Each bar represents the mean ± SD (error bars). $n = 2$ independent experiments. ACTB (β-actin) was used as a loading control.

http://dx.doi.org/10.1016/j.heliyon.2015.e00046

$SOX17^+FOXA2^+$ cells which represent DE progenitors. Using this method we found that, similar to mesoderm differentiation, DE differentiation efficiencies also highly depended upon the initial plating densities, and lower densities again gave rise to higher differentiation efficiencies (Fig. 4B). The highest differentiation efficiencies induced by the AWS condition were given by cells plated at 0.25×10^5 cells/cm^2 (36.1 ± 26.2%; Fig. 4B).

We then added MEG to the AWS condition either by pre-treatment (Fig. 4A; "MEG->AWS" or "pre-treatment" condition) or in combination with the growth factors (Fig. 4A; "MEG+AWS" or "combination" condition). Both approaches significantly boosted differentiation efficiencies for all plating densities tested (Fig. 4B). Most notably, both treatments dramatically enhanced the differentiation efficiency at the density of 1.0×10^5 cells/cm^2, from 11.8 ± 8.7% $SOX17^+FOXA2^+$ for the AWS condition, to an average of 72.7 ± 19.7% for the combination condition and 85.9 ± 6.1% for the pre-treatment condition (Fig. 4B). In some experiments, MEG treatments dramatically enhanced the efficiencies of DE progenitor differentiation to >90% under this optimum plating density, as shown by FACS analysis (Fig. 4C). A time course analysis of the MEG->AWS condition by immunofluorescence staining of SOX17 and FOXA2 is shown in Fig. 4D, again demonstrating a nearly homogeneous $SOX17^+FOXA2^+$ culture on day 7. The expressions of several other endoderm-specific markers including CER1, GATA4, GATA6, and GSC were also significantly enhanced by MEG, as shown by Western blotting (Fig. 4E) and qPCR (Fig. 4F). It should be noted that SOX17, FOXA2, and all the other endoderm markers discussed so far are pan-endoderm markers that are expressed in both definitive and extra-embryonic endoderm lineages (Borowiak et al., 2009). To rule out the possibility of extra-embryonic endoderm (ExEn) differentiation in this method, we examined the expressions of ExEn-specific markers AFP (α-fetoprotein) and SOX7 using Western blotting (Fig. 4E) and qPCR (Fig. 4F). Results showed no significant elevation of AFP and SOX7 in all differentiation conditions examined (Fig. 4E and F), verifying the DE-lineage identity of the differentiated progenies.

Similar to mesoderm-differentiation analyses, undifferentiated hESCs stained for SOX17 and FOXA2, instead of isotype IgG controls, were used as gating controls to prevent false positive measurement of the differentiation efficiency (46.74% false positive $SOX17^+FOXA2^+$ were detected if gate was setup by isotype IgG controls; Fig. 5A and Materials and Methods). A similar DE differentiation-enhancing effect of MEG was observed in the hiPSC line MMW2 (Fig. 5B). Moreover, MEG also improved the efficiencies of variations of DE induction conditions adopted from published protocols with modifications, such as AW-B27 (Norrman et al., 2013) (serum replaced by B-27 supplement; Fig. 5C) and AW-ITS (Cai et al., 2007) (serum replaced by ITS supplement; Fig. 5D) conditions (Materials and Methods).

http://dx.doi.org/10.1016/j.heliyon.2015.e00046

http://dx.doi.org/10.1016/j.heliyon.2015.e00046

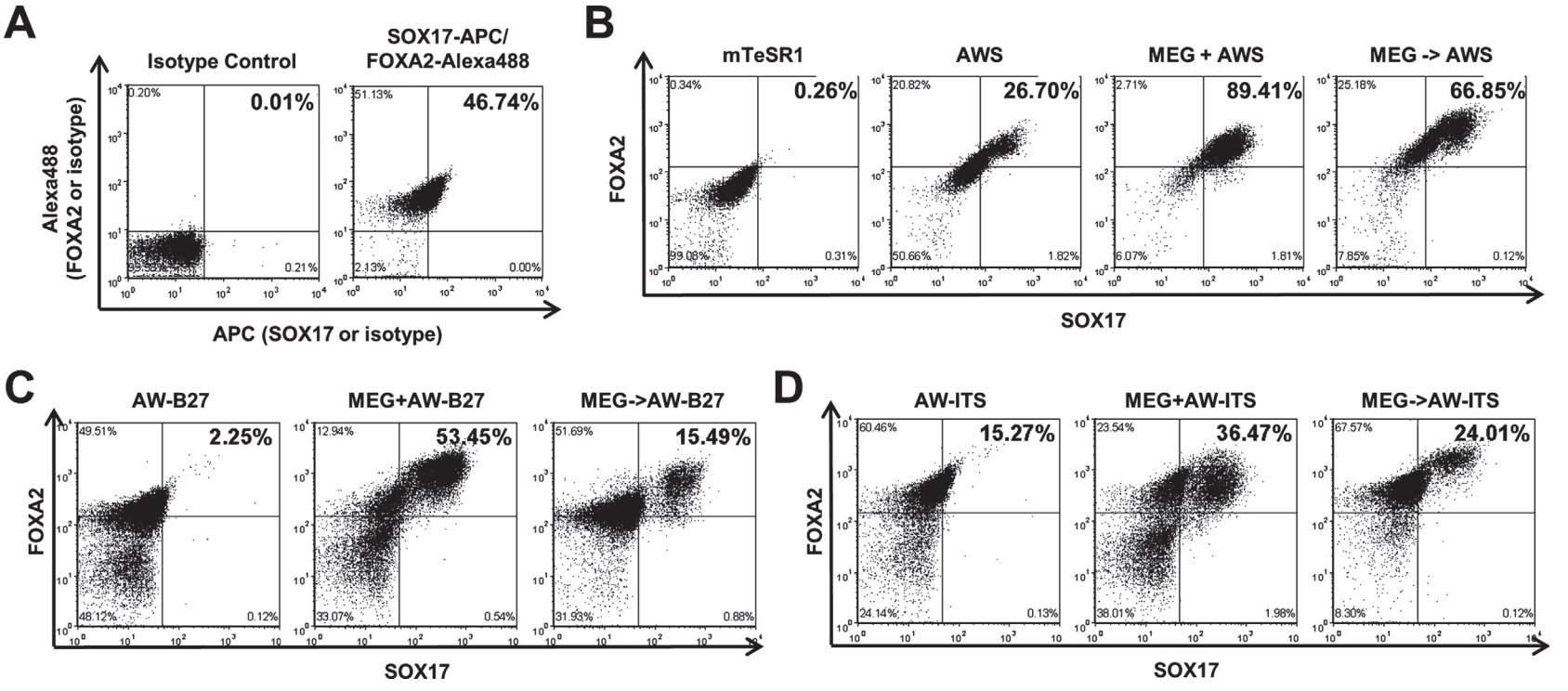

Fig. 5. MEG enhances definitive endoderm differentiation of hiPSCs and of variations of definitive endoderm induction conditions. (A) FACS analysis of SOX17 and FOXA2 in H9 hESCs cultured in mTeSR1 medium. Cells were stained with SOX17-APC and FOXA2-Alexa488 antibodies (SOX17-APC/FOXA2-Alexa488) or non-specific IgG isotype control antibodies conjugated with the same fluorophores (isotype control). Isotype IgG, when used as a gating control, gave rise to a high percentage of false-positive cells in the undifferentiated mTeSR1 culture (~50% APC^+/$Alexa488^+$ and ~98% $Alexa488^+$ in the SOX17-APC/FOXA2-Alexa-488 stained sample). $n > 10$ independent experiments. (B) FACS analysis of SOX17 and FOXA2 in MMW2 hiPSCs cells induced to undergo definitive endoderm differentiation under AWS, MEG+AWS, and MEG->AWS conditions for 7 days. Cells were plated at 1.0×10^5 cells/cm^2 for AWS and MEG+AWS conditions, and at 0.5×10^5 cells/cm^2 for MEG->AWS condition. Cells cultured in mTeSR1 medium were used as a gating control. $n = 2$ independent experiments. (C) FACS analysis of SOX17 and FOXA2 in H9 hESCs induced to undergo definitive endoderm differentiation for 5 days in AW-B27, MEG+AW-B27, and MEG->AW-B27 conditions. B-27 supplement was used in these conditions instead of serum. Cells were plated at 1.0×10^5 cells/cm^2. $n > 3$ independent experiments. (D) FACS analysis of SOX17 and FOXA2 in H9 hESCs induced to undergo definitive endoderm differentiation for 5 days in AW-ITS, MEG+AW-ITS, and MEG->AW-ITS conditions. ITS (insulin, transferrin, and selenium) supplement was used in these conditions instead of serum. Cells were plated at 2.0×10^5 cells/cm^2. $n = 2$ independent experiments.

2.4. MEG functions at the onset of mesoderm and DE differentiations but with no effect observed on Nodal and Wnt signaling

Based on the results that the pre-treatment conditions of MEG in both mesoderm and DE differentiations gave rise to similar, if not better, differentiation efficiencies compared to the combination conditions, we hypothesized that MEG may function by triggering a pathway (or pathways) involved only in the very early phase of mesoderm and DE inductions. Indeed, for both MEG+A-BVF (Fig. 6A) and MEG+AWS (Fig. 6B) conditions, the differentiation-enhancing effects of MEG were nearly completely lost when MEG was added starting from day 1 of differentiation instead of from day 0, strongly supporting this hypothesis.

As MEG enhances both mesoderm and DE differentiations, we further hypothesized that the biological pathway targeted by MEG may be involved in the developmental stage immediately upstream of mesoderm and DE specifications, namely primitive streak formation. As Nodal/TGF-β signaling pathway and canonical Wnt pathway are known to be essential for primitive streak induction (Conlon et al., 1994; Liu et al., 1999), we set out to examine the effect of MEG on these pathways. Overnight incubation of MEG was applied to mimic the pre-treatment conditions for mesoderm and DE differentiations. To test the effect of MEG on Nodal/TGF-β pathway, Activin A was added for various lengths of time after overnight incubation of MEG. Pre-treatment of MEG at a wide range of doses all failed to vary the signaling strength of Nodal/TGF-β pathway, quantified by the level of Phospho-SMAD2 (Fig. 6C). A time course analysis after overnight incubation and with continues addition of MEG during Activin A treatment also showed no effect of MEG on the maintenance of Nodal/TGF-β signaling over time (Fig. 6D). On the other hand, overnight treatment of MEG showed no effect on the activation of canonical Wnt signaling pathway, quantified by the level of Phospho-β-CATENIN (Fig. 6E).

2.5. *In vitro* kinome screen and functional validations identified TRPM6 as the biological target of MEG

To investigate the molecular mechanism of MEG, we employed a series of target identification and validation techniques. We first conducted structure-activity relationship (SAR) assays, a technique used to determine structural module(s) within a bioactive small molecule that is/are responsible for its biological activity and to identify the overall chemical structure which possesses the strongest bioactivity. In brief, a number of structurally similar compounds with the same basic chemical backbone but modified by different side groups at

http://dx.doi.org/10.1016/j.heliyon.2015.e00046

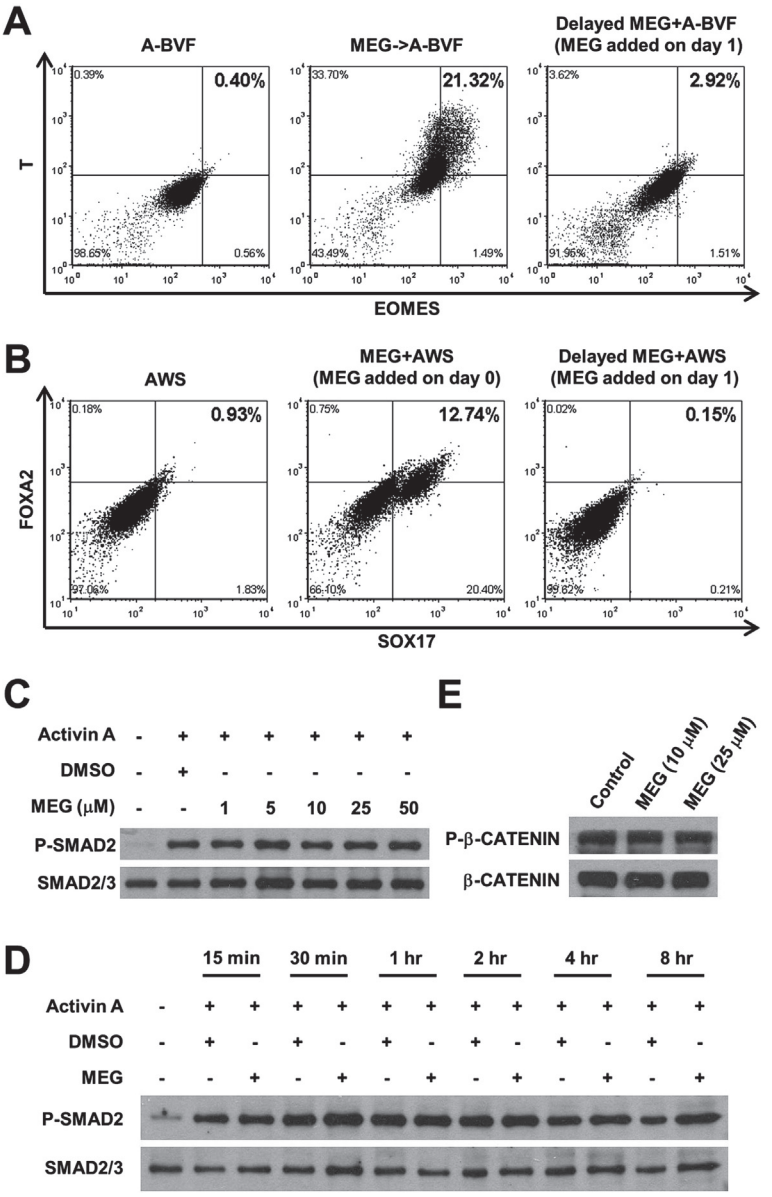

Fig. 6. MEG functions at the onset of mesendoderm differentiation but shows no effect on Nodal and Wnt signaling. (A) FACS analysis of T and EOMES in H9 hESCs differentiated in MEG-> A-BVF, A-BVF, and delayed MEG+A-BVF (with MEG added on day 1 instead of day 0) conditions. (B) FACS analysis of SOX17 and FOXA2 in H1 hESCs differentiated for 7 days in AWS condition and MEG+AWS condition with MEG added on day 0 or day 1. Cells were plated at 1.5×10^5 cells/cm^2. (C) Western blotting of Phospho-SMAD2 (P-SMAD2) in H1 hESCs pre-treated with DMSO and MEG in mTeSR1 medium overnight, followed by 0.5 hr treatment of Activin A (10 ng/ml) in RPMI-1640 medium. SMAD2/3 was used as a loading control. $n = 3$ independent experiments. (D) Western blotting of Phospho-SMAD2 (P-SMAD2) in H1 hESCs untreated or pre-treated with DMSO and MEG (10 μM) in mTeSR1 medium overnight, followed by treatment of Activin A (10 ng/ml) in RPMI-1640 medium with DMSO and MEG for various lengths of time. SMAD2/3 was used as a loading control. (E) Western blotting of Phospho-β-CATENIN (P-β-CATENIN) in H1 hESCs untreated (Control) or treated with MEG at 10 μM and 25 μM in mTeSR1 medium overnight. β-CATENIN was used as a loading control. $n = 2$ independent experiments.

http://dx.doi.org/10.1016/j.heliyon.2015.e00046

different positions (serially numbered as MEG analogs (MA) 1–12; Fig. 7A shows the closest analogs of MEG, whereas Fig. 7B shows the more distant analogs) were purchased and assayed side-by-side with MEG under differentiation conditions for their differentiation-enhancing capabilities. Mesoderm differentiation was used for the tests as its duration is significantly shorter than DE differentiation. At 5 μM two structural analogs of MEG, MA1 and MA2, showed observable enhancement effects on mesoderm differentiation, although insignificant compared to the effect of MEG tested alongside at 1 μM (Fig. 8A); none of the other structural analogs tested showed significant enhancement effect at 5 μM (Fig. 8A). Both MA1 and MA2 showed stronger effects when tested at a higher dose of 20 μM, confirming their differentiation-enhancing activities, although MEG was still the most active at 10 μM (Fig. 8B). Both compounds and MEG share a $-C(CH_3)_2$ group at position R^3 of their structures, which appears to be a crucial side group for their activities as compound MA4, missing only the $-C(CH_3)_2$ group compared to MEG, showed

A

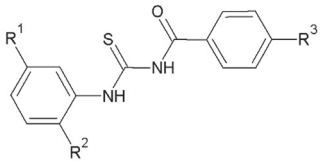

Compound No.	ChemBridge Compound ID	R^1	R^2	R^3
MEG	6528694	CF_3	Cl	$C(CH_3)_2$
MA1	6512888	CF_3	×	$C(CH_3)_2$
MA2	6538520	×	×	$C(CH_3)_2$
MA3	6591822	×	OH	$C(CH_3)_2$
MA4	6419968	CF_3	Cl	×
MA5	5562754	×	OH	×

B

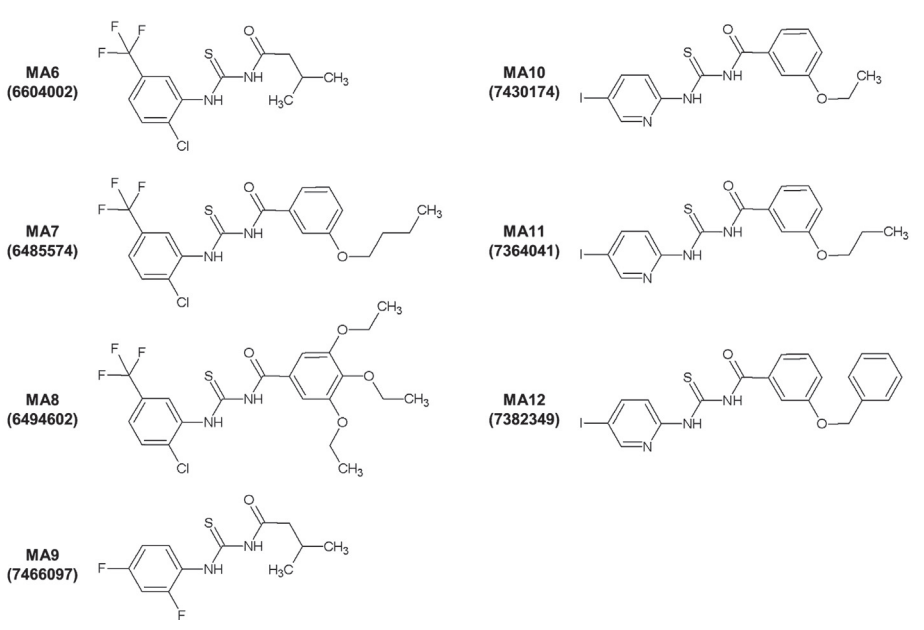

Fig. 7. Structural analogs of MEG. (A) Basic chemical structures of MEG and its close analogs (MA1–MA5). Labels R^1, R^2, and R^3 mark the positions of chemical groups that modify the backbone structure shared by the analogs. (B) Chemical structures for MEG analogs 6–12 (MA6–MA12) tested in SAR analysis.

http://dx.doi.org/10.1016/j.heliyon.2015.e00046

http://dx.doi.org/10.1016/j.heliyon.2015.e00046

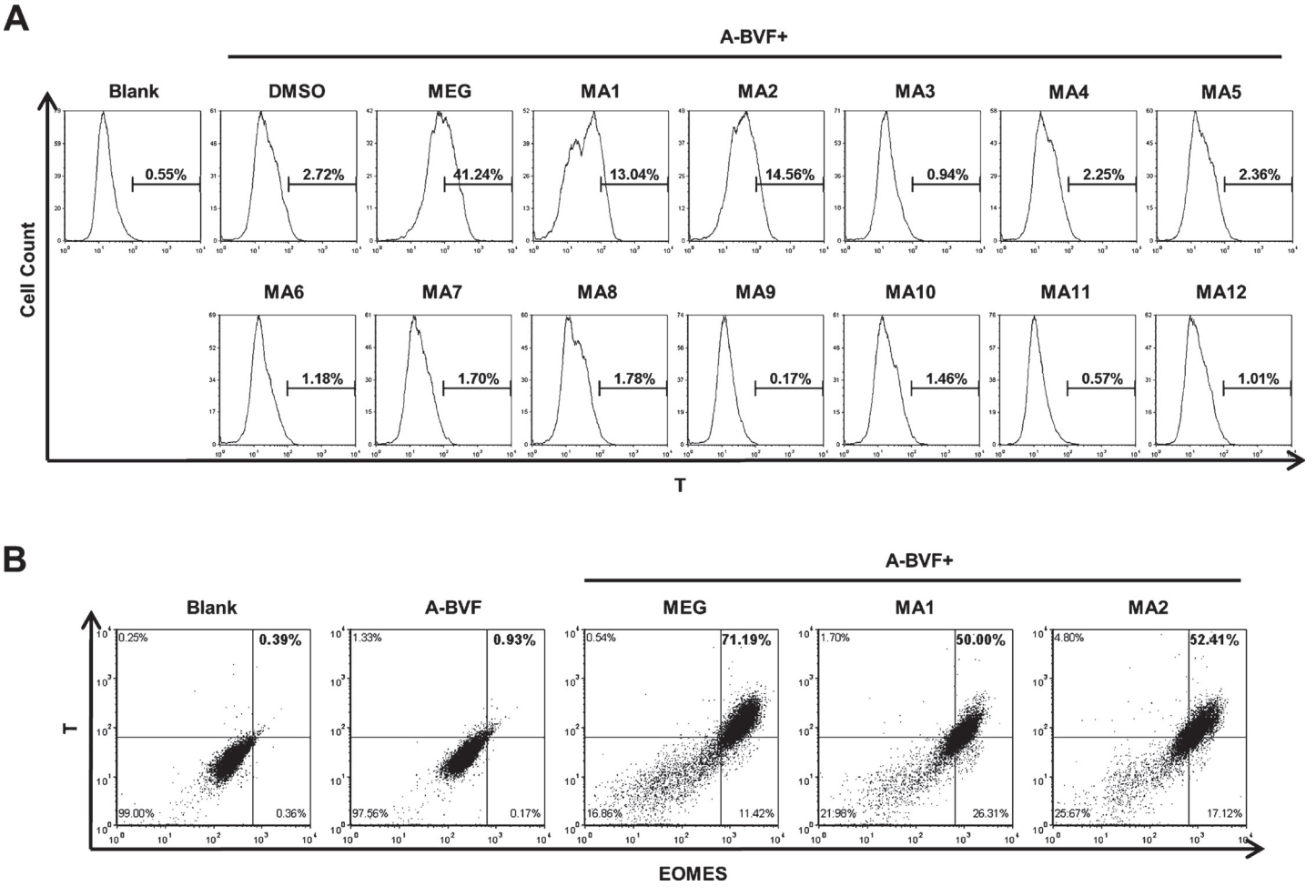

Fig. 8. SAR analysis identified MEG as the most potent compound among close structural analogs. (A) FACS analysis of T in H9 hESCs differentiated for 2 days in A-BVF condition in combination with DMSO, MEG (1 μM), or chemical analogs of MEG (5 μM, except 1 μM for MA12). Cells maintained in basal differentiation medium for 2 days but without the addition of growth factors (Blank) generally show similar levels of background signals for T and EOMES stainings as in undifferentiated hESCs (data not shown) and were used as a gating control. $n = 2$ independent experiments. (B) FACS analysis of T and EOMES in H9 hESCs differentiated for 2 days in A-BVF condition with or without MEG (10 μM), MA1 (20 μM), and MA2 (20 μM). Cells maintained in basal differentiation medium but without the addition of growth factors (Blank) were used as a gating control. $n = 2$ independent experiments.

no differentiation-inducing capability under the condition tested (Fig. 8A). On the other hand the $–CF_3$ and –Cl groups at positions R^1 and R^2, respectively, could be removed while keeping a significant part of MEG's bioactivity (MA1 and MA2; Fig. 8A and B), although interestingly, adding back a –OH group at R^2 seemed to have abolished the remaining activity of MA2 (MA3; Fig. 8A). Because results from SAR analysis showed that MEG remains to be the most potent molecule within all of its commercially available structural analogs, we decided to continue using MEG for all subsequent target identification and validation experiments.

Kinases are important regulators of biological pathways and are involved in a wide variety of biological processes; their roles during cellular differentiation and embryonic development are being actively studied (Choi et al., 2007; Oh et al., 2009; Tian et al., 2009). The enzymatic activities of kinases can be inhibited at their ATP-binding sites by small planar compounds with high aromatic contents but no stereocenters (Huigens et al., 2013), which are characteristics shared by MEG. We thus postulated that MEG may function by targeting ATP-binding site-containing proteins such as kinases, and applied MEG to an *in vitro* kinase screen using a commercial service (KINOMEscan by DiscoveRx; Materials and Methods). A total of 456 kinases were analyzed with results summarized in Fig. 9A, in which a lower Percent-of-Control (%Ctrl) value indicates a stronger interaction between the test compound and a kinase. Only two kinases gave %Ctrl values lower than 60, with a %Ctrl value of 50 for TRPM6 and 47 for NEK3 (Fig. 9B). The TRPM7 channel kinase was not included in this screen.

As numerous studies have indicated a potential regulatory role of TRPM6/TRPM7 channels during embryonic development, we hypothesized that TRPM6 may be the biological target of MEG. To test this hypothesis we first confirmed the expression of TRPM6 in undifferentiated hESCs. *TRPM6* gene encodes 7 isoforms via alternative splicing, with isoforms TRPM6a, TRPM6b, and TRPM6c containing the transmembrane channel domain and the kinase domain, isoforms TRPM6-kinase-1, -2, and -3 containing only the kinase domain, and the testes-specific isoform TRPM6t containing only the transmembrane domain (Chubanov et al., 2004). RT-PCR analysis using isoform-specific primers (Chubanov et al., 2004) showed that the kinase- and channel domain-containing isoforms *TRPM6a* and *TRPM6b*, but not the other isoforms of *TRPM6*, were expressed in undifferentiated hESCs (Fig. 9C). *TRPM7*, the ubiquitously expressed member of the TRPM protein family (Chubanov et al., 2005a), was also expressed in hESCs as expected (Fig. 9C).

We then tested whether the inhibition of TRPM6 expression can mimic the effect of MEG on hESC differentiation. As prolonged depletion of cellular Mg^{2+}

http://dx.doi.org/10.1016/j.heliyon.2015.e00046

by a persistent TRPM6 knock down during differentiation will ultimately lead to cell death, to avoid the selective loss of TRPM6 knock-down cells during differentiations and thus inaccurate measurements of the differentiation efficiencies, we delivered the shRNA constructs by transient transfections rather than stable lentiviral infections at the beginning of each experiment.

A

Percent of Control (%Ctrl)	90 - 100	80 - 90	63 - 80	≤ 50
Number of kinases within each range of %Ctrl	365	64	25	2

B

Hit kinase	%Ctrl
TRPM6	50
NEK3	47

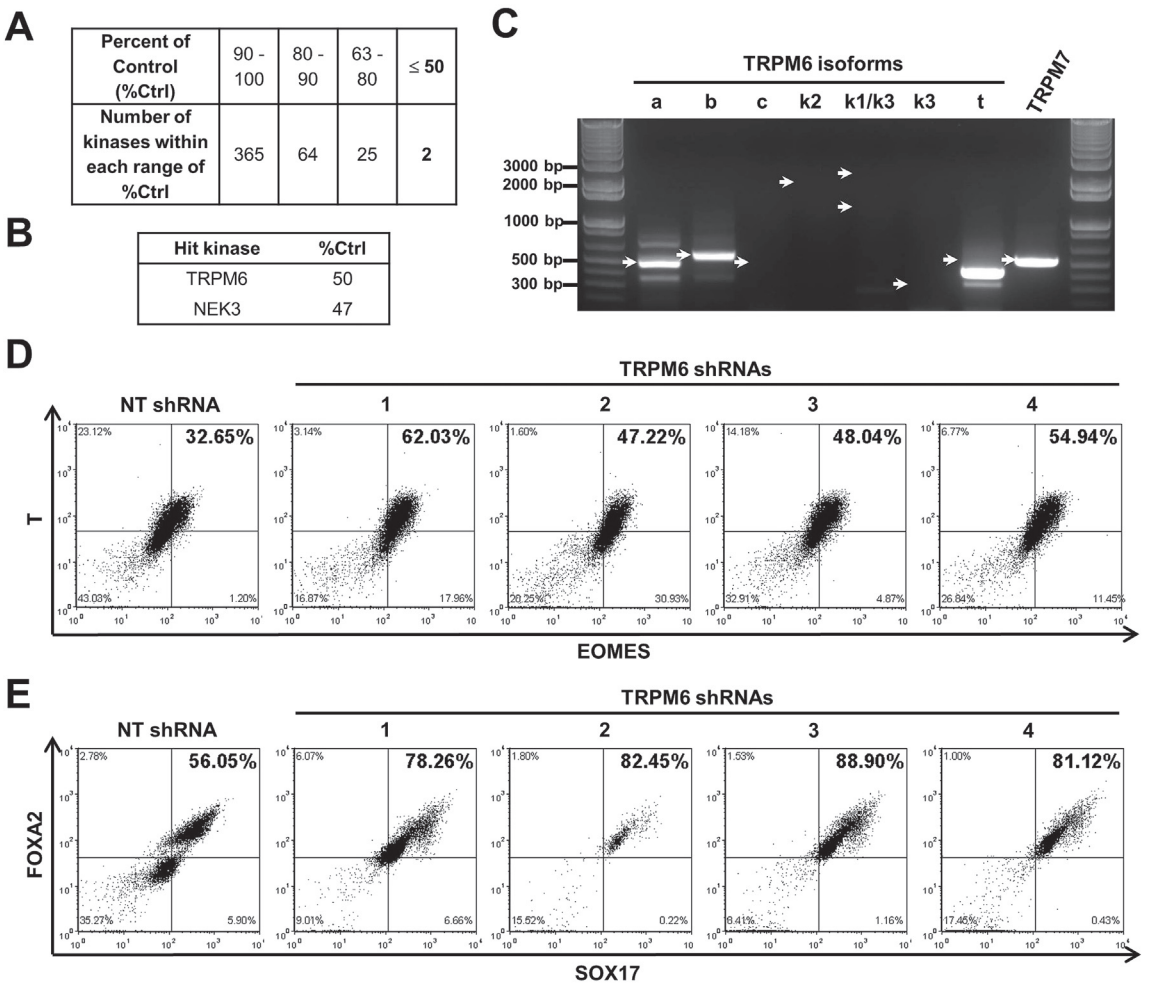

Fig. 9. TRPM6 is the biological target of MEG. (A) Summary of KINOMEscan result. Lower values of %Ctrl indicate stronger interactions between the test compound and the kinases. (B) %Ctrl values for TRPM6 and NEK3 as detected in KINOMEscan. (C) Agarose gel electrophoresis showing RT-PCR amplification of undifferentiated H1 hESCs using TRPM6 isoform-specific PCR primers. White arrows point to the expected positions of the amplified bands. Note that the band shown in the "t" lane is not in the correct position and thus does not indicate expression of the t isoform. a: TRPM6a; b: TRPM6b; c: TRPM6c; k1: TRPM6-kinase-1; k2: TRPM6-kinase-2; k3: TRPM6-kinase-3; t: TRPM6t. (D) FACS analysis of T and EOMES in H9 hESCs transfected with NT shRNA and TRPM6 shRNAs and differentiated under A-BVF condition for 2 days. $n = 4$ independent experiments. (E) FACS analysis of SOX17 and FOXA2 in H1 hESCs treated with NT shRNA and TRPM6 shRNAs and differentiated under AWS condition for 7 days. $n = 3$ independent experiments.

http://dx.doi.org/10.1016/j.heliyon.2015.e00046

The fact that MEG functions specifically at the start of differentiation inductions (Fig. 6A and B) also indicated that a transient knock down of the true biological target of MEG, even if only during the onset of differentiation, should be sufficient to phenocopy MEG, and should also represent a more stringent test for the biological relevance of the target. A recently published method which greatly boosted transient transfection efficiencies in hESCs by the use of ROCK inhibitor Y-27632 has been applied to our experiments (Yen et al., 2014) (Materials and Methods). As a result, TRPM6 knock down significantly enhanced the efficiencies of both mesoderm (Fig. 9D) and DE (Fig. 9E) differentiations, whereas NEK3 knock down failed to offer any significant enhancement effect in growth factor-induced mesoderm (Fig. 10A) and DE (Fig. 10B) differentiations. These results, from a phenotypical standpoint, confirmed that TRPM6 rather than NEK3 is most likely to be the biological target of MEG.

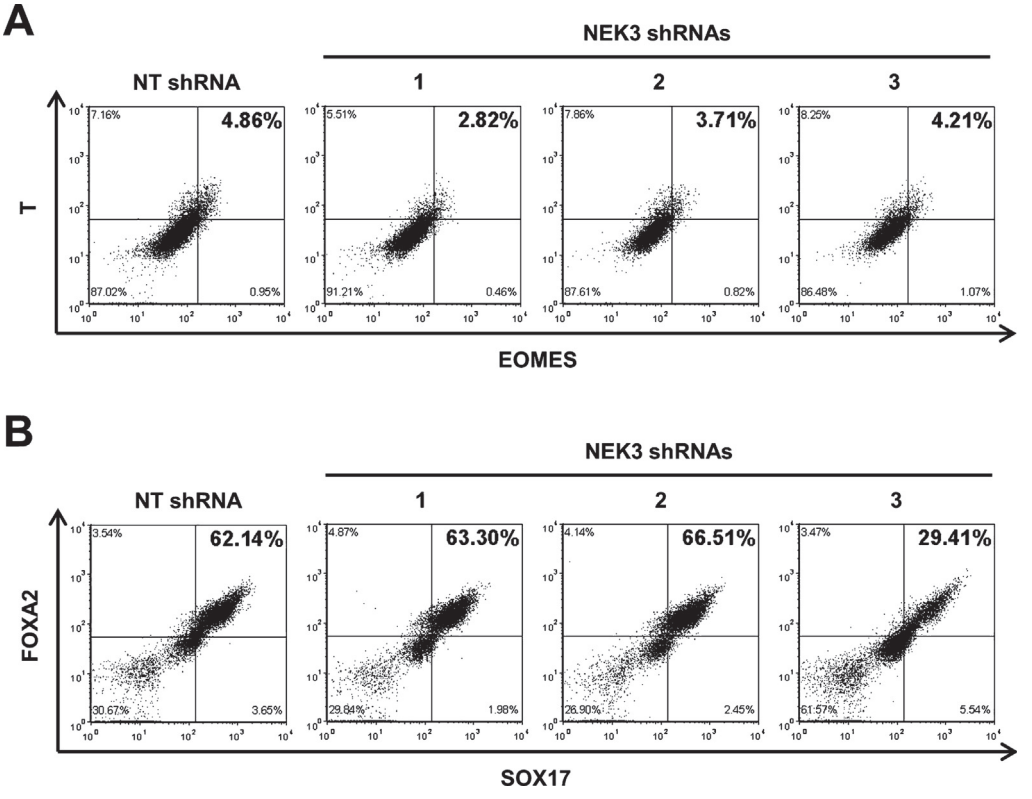

Fig. 10. NEK3 is not the biological target of MEG. (A) FACS analysis of T and EOMES in H1 hESCs transfected with NT shRNA and NEK3 shRNAs and differentiated under A-BVF condition for 2 days. Cells were plated at 0.5×10^5 cells/cm^2. Cells cultured in mTeSR1 medium were used as a gating control. $n = 4$ independent experiments. (B) FACS analysis of SOX17 and FOXA2 in H1 hESCs transfected with NT shRNA and NEK3 shRNAs and differentiated under AWS condition for 7 days. Cells were plated at 1.0×10^5 cells/cm^2. Cells cultured in mTeSR1 medium were used as a gating control. $n = 2$ independent experiments.

http://dx.doi.org/10.1016/j.heliyon.2015.e00046

2.6. Inhibitions of TRPM6/TRPM7 channel activity and cellular Mg^{2+} uptake mimic the biological effect of MEG

As the best understood biological function of TRPM6 is in magnesium ion transportation (Chubanov et al., 2005b; Chubanov et al., 2004; Schlingmann et al., 2007), we set out to investigate the effect of MEG on cellular magnesium homeostasis. Indeed, overnight incubation of MEG dramatically reduced intracellular magnesium level in a dose dependent manner, as shown by flow cytometry analysis using a magnesium sensor Mag-fluo-4 as indicator (Fig. 11A). We thus hypothesized that MEG functions by inhibiting the magnesium transport activity of TRPM6/TRPM7 channel, and tested this hypothesis by examining whether other known TRPM6/TRPM7 channel modulators or Mg^{2+}-withdrawal can phenocopy MEG.

As a result, TRPM6/TRPM7 channel blocker Ruthenium Red (RR; 50 μM) and modulator 2-aminoethoxydiphenyl borate (2-APB) (50 μM) significantly enhanced mesoderm differentiation efficiency to a degree comparable to what was observed in MEG (10 μM) treated samples (Fig. 11B); similar results were obtained in DE differentiation (Fig. 11C). Note that the channel modulator 2-APB is known to increase TRPM6 but inhibit TRPM7 homo-tetrameric channel activity at the micromolar level (Li et al., 2006), suggesting that the inhibition of TRPM7 channel activity may have contributed more to the biological phenotypes caused by MEG than TRPM6 channel inhibition. Meanwhile, withdrawal of Mg^{2+} in mesoderm differentiation medium dramatically enhanced growth factor-induced mesoderm differentiation to a degree greater than that achieved by MEG treatment alone (74.3% versus 42.1% T^+EOMES^+), whereas the combined treatment of MEG failed to further enhance mesoderm differentiation efficiency on top of Mg^{2+}-withdrawal (73.4% versus 74.3% T^+EOMES^+) (Fig. 11D), indicating that withdrawal of Mg^{2+} not only phenocopied MEG but also rendered MEG-treatment ineffective for further mesodermal induction. Similar results were observed in DE differentiation, with Mg^{2+}-withdrawal only during the first day of differentiation significantly boosted the overall efficiency from 49.8% to 75.9% $SOX17^+FOXA2^+$ (Fig. 11E). Adding excess amount of Mg^{2+} in the differentiation medium to up to 10 mM final concentration modestly reversed the differentiation enhancing effects of MEG in both mesoderm (Fig. 11F) and DE (Fig. 11G) differentiations, although never completely back to the same level as in the control samples. Together these results demonstrated that MEG most likely exerts its biological function by modulating TRPM6/TRPM7 channel activities and, subsequently, cellular magnesium homeostasis.

Notably, both channel modulators and MEG significantly inhibited neural differentiation activity induced by Dorsomorphin, a dual inhibitor of Nodal and

http://dx.doi.org/10.1016/j.heliyon.2015.e00046

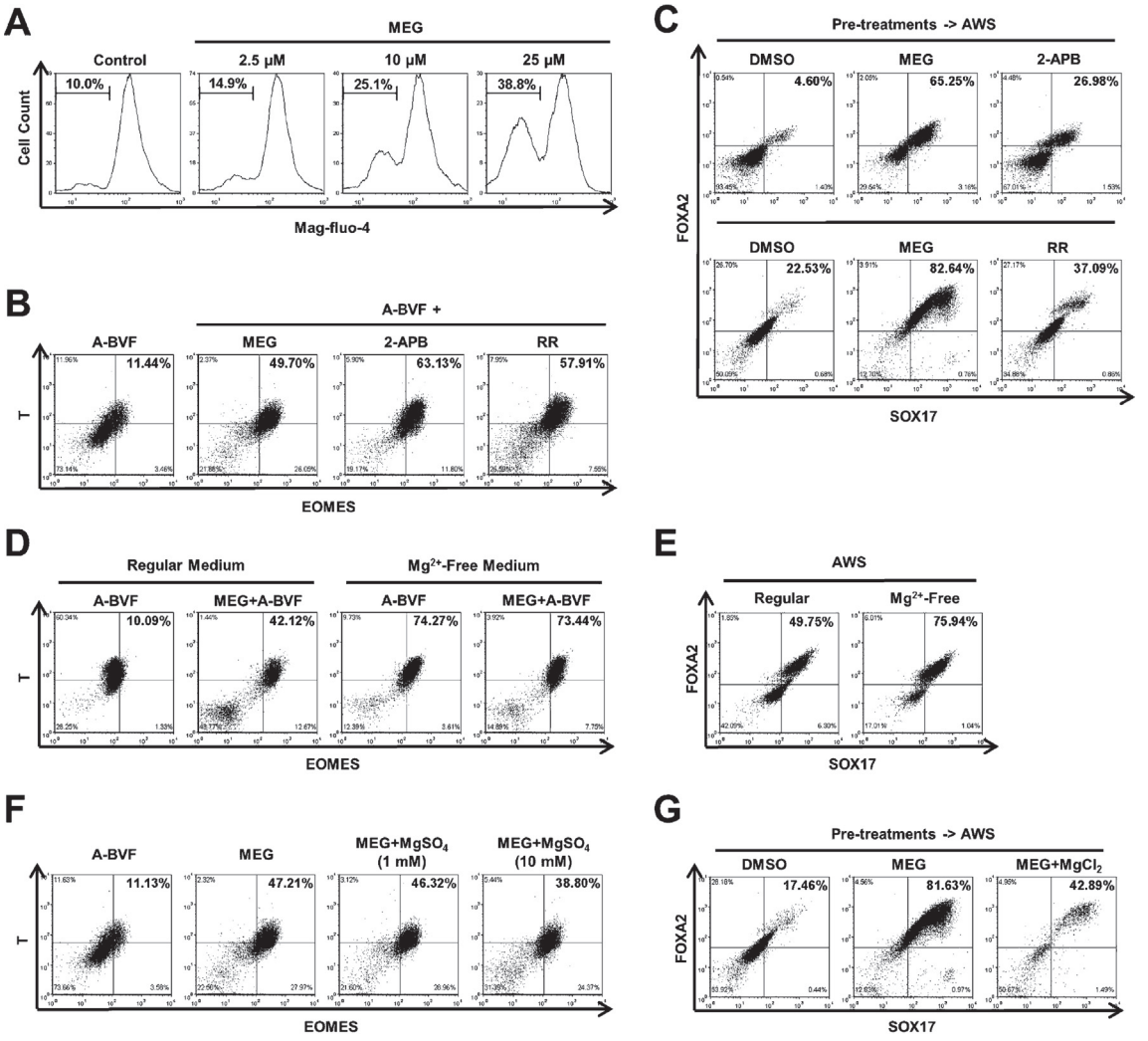

Fig. 11. MEG functions by inhibiting cellular magnesium uptake. (A) FACS analysis of magnesium sensor Mag-fluo-4 in H1 hESCs untreated (Control) or treated with various doses of MEG overnight in mTeSR1 medium. $n = 3$ independent experiments. (B) FACS analysis of T and EOMES in H1 hESCs differentiated under A-BVF condition for 2 days with or without the addition of MEG (10 μM), 2-APB (50 μM), and Ruthenium Red (RR; 50 μM). Cells were plated at 0.5×10^5 cells/cm^2. $n = 4$ independent experiments. (C) FACS analysis of SOX17 and FOXA2 in two independent experiments of H1 hESCs pre-treated with DMSO, 10 μM MEG, and 50 μM 2-APB (top panel), and DMSO, 10 μM MEG, and 10 μM Ruthenium Red (RR) (bottom panel), followed by DE differentiation under AWS condition for 7 days. $n = 3$ independent experiments. (D) FACS analysis of T and EOMES in H1 hESCs differentiated under A-BVF condition with or without MEG (10 μM) in regular medium or Mg^{2+}-free medium for 2 days. $n = 3$ independent experiments. (E) FACS analysis of SOX17 and FOXA2 in H1 hESCs differentiated under AWS condition for 7 days in regular medium or Mg^{2+}-free medium. $n = 3$ independent experiments. (F) FACS analysis of T and EOMES in H1 hESCs differentiated under A-BVF condition for 2 days with or without the addition of MEG (10 μM) and MEG+$MgSO_4$ (1 mM and 10 mM). Cells were plated at 0.5×10^5 cells/cm^2. $n = 2$ independent experiments. (G) FACS analysis of SOX17 and FOXA2 in H1 hESCs pre-treated with DMSO, MEG (10 μM), and MEG+$MgCl_2$ (10 mM) followed by AWS differentiation for 7 days. $n = 2$ independent experiments.

http://dx.doi.org/10.1016/j.heliyon.2015.e00046

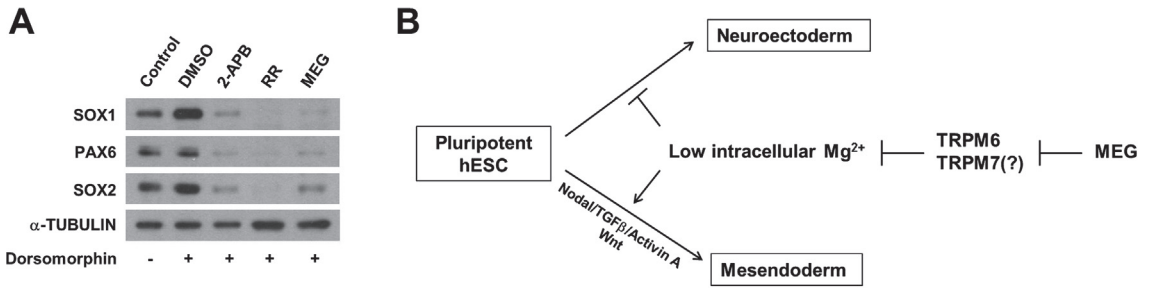

Fig. 12. A working model for a potential role of magnesium during cell fate specification. (A) Western blotting of neural progenitor markers SOX1, PAX6, and SOX2 in H1 hESCs cultured in neural differentiation medium for 7 days untreated (Control) or treated with Dorsomorphin (1 μM). The Dorsomorphin treated samples were also incubated with DMSO, 2-APB (50 μM), Ruthenium Red (RR; 50 μM), and MEG (10 μM), respectively. α-TUBULIN was used as a loading control. $n = 3$ independent experiments. (B) Schematic representation of a working model summarizing the findings of this study and suggesting a potential role of magnesium during cell fate specification.

BMP pathways (Zhou et al., 2010) (Materials and Methods) (Fig. 12A). This result indicates that cellular magnesium level may have a differential regulatory effect on neural differentiation as compared to mesoderm and DE differentiations; specifically, a low level of cellular Mg^{2+} may be favorable to mesendoderm differentiation while inhibitory to neuroectoderm differentiation (Fig. 12B).

3. Discussion

In summary, this study demonstrated the nearly homogeneous derivations of mesoderm and DE progenitors from hESCs enhanced by a novel small molecule inhibitor MEG. Further investigations indicated that MEG performs its biological function by targeting TRPM6/TRPM7 channels and subsequently regulating cellular magnesium level, shedding light on a novel function of magnesium during early embryonic development.

Extensive efforts were taken in this study to scrutinize the identities of the differentiated progenies and to ensure accurate measurements of the differentiation efficiencies in this study.Intracellular FACS staining of lineage-specific markers, arguably one of the most accurate and discriminative method available for cell-fate validation at the single cell level, was used as the primary method in this study to distinguish and quantify the productions of mesoderm and DE progenitors. As a technical note, many of the experiments conducted for the mechanism study of MEG were not performed under optimum plating densities for the A-BVF- and AWS-only conditions as determined in this report (Figs. 2B and 4B); rather they were optimized for MEG and other treatment conditions in such a way that the differentiation-enhancing effects of these treatments over the growth factor-only conditions could be more clearly observed.

http://dx.doi.org/10.1016/j.heliyon.2015.e00046

As MEG reduces intracellular level of Mg^{2+} (Fig. 11A), a cation essential for normal cellular functions, it is worth examining whether MEG treatment leads to cellular stress or toxicity. In our hands, we found that the cytotoxicity level of MEG depended on several factors including plating density of the cells, culture condition, treatment duration, and dosage. In general, MEG showed higher toxicities when added to cells plated at lower densities. This density-dependent toxicity was especially evident under DE induction condition; in fact, MEG often caused non-negligible levels of toxicity to cells plated at or below 0.5×10^5 cells/cm^2 for the pre-treatment condition, and for cells plated at 0.25×10^5 cells/cm^2 for the combination condition of DE induction, giving rise to large experimental variations, which was why these data points were excluded from the summary table for DE induction efficiencies (Fig. 4B). Compared to the DE induction condition, the mesoderm induction condition had shown a much higher level of tolerance to MEG. MEG only started to show a non-ignorable level of cytotoxicity at the lowest plating density tested (0.1×10^5 cells/cm^2) for mesoderm induction; it was also for this reason that this data point was omitted from the mesoderm differentiation summary table (Fig. 2B). The reason for this differential tolerance between mesoderm and DE induction conditions is unknown. Predictably, prolonged treatments of MEG caused higher levels of cytotoxicity; it was due to this reason that the dosage of MEG was reduced to 1 μM for the combination condition of DE induction to accommodate the longer treatment duration (7 days; Materials and Methods).

The exact mechanism of the molecular interaction between MEG and TRPM6 remains to be elucidated. As the kinases were bound by a non-specific kinase inhibitor targeting their ATP-binding sites in the kinome screen, MEG may have released TRPM6 by directly (sterically) competing with the ligand at its ATP-binding site or by acting as an allosteric inhibitor. In depth biochemical or computational analyses are granted to further characterize the nature of this interaction. On the other hand, although TRPM7 was not included in the kinome screen, it may also be a target of MEG due to its high sequence similarity with TRPM6 (77%) (Nilius and Flockerzi, 2014). In fact, the result that the channel modulator 2-APB, a potentiator of TRPM6 but an inhibitor of TRPM7 homo-tetrameric channel activity at the micromolar level (Li et al., 2006), phenocopied MEG at a concentration of 50 μM, suggests that the inhibition of TRPM7 channel activity may have contributed more to the biological function of MEG than TRPM6 channel inhibition. The kinase domains of TRPM6 and TRPM7 have both been reported to have regulatory roles over TRPM6/TRPM7 channel activities (Nilius and Flockerzi, 2014), which could offer an explanation for the mechanism of action of MEG.

By studying the molecular mechanism underlying the function of MEG, we have demonstrated a regulatory role of intracellular Mg^{2+} homeostasis during

http://dx.doi.org/10.1016/j.heliyon.2015.e00046

early embryonic cell fate determination in an *in vitro* cell culture system. Despite limitations of an *in vitro* system, our findings may still offer insights into the study of embryonic development *in vivo*. On the one hand, the fact that MEG, TRPM6/TRPM7 channel blockers, and magnesium-withdrawal simultaneously enhanced the inductions of both mesoderm and DE, the two daughter lineages of primitive streak, indicates that a low intracellular level of magnesium may be favorable to primitive streak formation during early development. The fact that delayed treatment of MEG was ineffective also indicates that this biological phenomenon may be most relevant during the earliest onset of primitive streak induction *in vivo*. On the other hand, the fact that MEG and the channel blockers inhibited neural differentiation (Fig. 12A) indicates that a higher intracellular magnesium level may be a prerequisite of neural induction. As briefly discussed in the Introduction, a previous study in *Xenopus laevis* concluded that the underlying cause of the neural tube closure defects induced by TRPM7 or Mg^{2+} depletion was the inhibition of noncanonical Wnt pathway (PCP pathway) (Liu et al., 2011). However, in an earlier work using mouse as a model (Walder et al., 2009), the authors claimed to have never seen "an embryo with complete absence of neural tube closure" in mice defective of TRPM6, and thus "the primary defect seems not to involve disordered planar cell polarity". Although still extremely preliminary, our result, from a stem cell biologist's point of view, offers an alternative perspective for the possible cause of this phenotype by showing that inhibition of cellular Mg^{2+} uptake may be, on a cellular level, inhibitory to neural differentiation (Fig. 12A). These theories will remain as speculations until carefully examined in an *in vivo* developmental system.

4. Materials and methods

4.1. Cell culture

H9 and H1 hESC lines (WiCell Research Institute, Madison, WI) and MMW2 hiPSCs (Mali et al., 2010) were maintained under a feeder condition or a feeder-independent condition. For the feeder condition (Thomson et al., 1998), primary mouse embryonic fibroblasts (MEFs) prepared from embryos of pregnant CF-1 mice (day 13.5 of gestation; Charles River) were cultured in DMEM containing 10% FBS (Hyclone), 1% non-essential amino acids (NEAA; Invitrogen), and penicillin/streptomycin, and mitotically inactivated by gamma irradiation. H9 and H1 hESCs and hiPSCs were cultured on irradiated MEFs in media containing DMEM/F12, 20% knockout serum replacement (KSR; Invitrogen), 4 ng/ml basic fibroblast growth factor (bFGF; Invitrogen), 1% NEAA, 1 mM glutamine, and 0.1 mM β-mercaptoethanol. For the feeder-independent condition, hESCs and hiPSCs were cultured on Matrigel (BD Biosciences)-coated plates in mTeSR1 medium (StemCell Technologies) as

http://dx.doi.org/10.1016/j.heliyon.2015.e00046

described (Ludwig et al., 2006). Experiments described in this study were conducted with H9 and H1 hESCs between passages 30 and 60.

4.2. Small scale screening of mesoderm and DE inducers

Previously a high-throughput chemical screening was conducted at the High-Throughput Screening Facility (HTSF) at the University of Illinois at Urbana−Champaign (http://www.scs.illinois.edu/htsf/index.html). A total of 171,077 compounds from the Marvel Library, the HTSF House Library, the ChemBridge MicroFormat Library, and the National Cancer Institute (NCI) library were screened, giving rise to 29 bioactive small molecules which potently disrupt hESC pluripotency (Geng et al., 2015). Using this collection of 29 bioactive compounds, we conducted the small scale screen for mesoderm and DE inducers. For this screen, hESCs were maintained in the pluripotent state in mTeSR1 medium (Ludwig et al., 2006). Small molecules were added at 1–10 μM, depending on their respective potencies and toxicities shown at the validation stage of the previous high-throughput screen (Geng et al., 2015), and incubated for 5–7 days to induce differentiation. Differentiated cultures were then assayed for mesoderm, DE, and neural lineage-specific marker expressions using Western blotting. Compounds that selectively induced the expressions of mesoderm and DE markers, but not neural markers, were identified as hits.

4.3. Mesoderm differentiation

To induce directed mesoderm differentiation, we used a growth-factor combination ("A-BVF"), as previously reported with modifications (Bernardo et al., 2011; Evseenko et al., 2010; Yu et al., 2011). H1 and H9 hESCs or MMW2 hiPSCs were dissociated by Accutase (Invitrogen) and seeded onto culture plates pre-coated with Matrigel (BD Biosciences) in mTeSR1 medium (StemCell Technologies) supplemented with Y-27632 (10 μM; Calbiochem). The day of seeding was referred to as "day -2". On day 0, mTeSR1 medium was replaced by a mesoderm induction medium, in which the basal medium (Advanced RPMI-1640 basal medium supplemented with B-27 and Glutamax; all from Invitrogen) was supplemented by Activin A (R&D Systems), BMP4 (Invitrogen), human VEGF (Invitrogen), and bFGF (Invitrogen) (all at 10 ng/ml) from day 0 to day 1, while Activin A was removed from this medium from day 1 to day 2. This protocol was referred to as the A-BVF condition.

For MEG induction, MEG was either added to the mTeSR1 medium on day "-1" as the "MEG->A-BVF" or "pre-treatment" condition (10 μM), or added to the mesoderm induction medium as the "MEG+A-BVF" or "combination"

http://dx.doi.org/10.1016/j.heliyon.2015.e00046

condition (1, 5, or 10 μM). Cells were collected on day 1.5 to day 2 of this protocol for further analyses.

Variations of mesoderm induction protocols used in this study include the "BVF" condition with BMP4 (10 ng/ml), VEGF (10 ng/ml), and bFGF (20 ng/ml), and the "BF" condition with BMP4 (10 ng/ml) and bFGF (20 ng/ml).

4.4. Definitive Endoderm differentiation

To induce definitive endoderm differentiation, we applied a method utilizing Activin A, WNT3A and low concentrations of fetal bovine serum (FBS) which was modified from previously reported methods (Borowiak et al., 2009; D'Amour et al., 2005). H1 and H9 hESCs or MMW2 hiPSCs were seeded in the same way as described for mesoderm differentiation, on day "-2". On day 0, mTeSR1 medium was replaced by an definitive endoderm induction medium, in which a basal medium (Advanced RPMI-1640 medium supplemented by Glutamax; Invitrogen) was supplemented by Activin A (50 or 100 ng/ml; from day 0 to day 7), WNT3A (25 ng/ml; from day 0 to day 1) (R&D Systems), 0.2% FBS (from day 1 to day 2), and 2% FBS (from day 2 to day 7). This protocol was referred to as the AWS condition.

For MEG induction, MEG was either added to the mTeSR1 medium at 10 μM on day "-1" as the "MEG->AWS" or "pre-treatment" condition, or added to the definitive endoderm induction medium at 1 μM throughout the course of differentiation as the "MEG+AWS" or "combination" condition. Cells were collected on day 5 of this protocol for qPCR analysis, and day 7 for Western blotting or FACS analysis.

Variations of DE induction protocols used in this study include the "AW-B27" condition in which FBS was replaced by 2% B-27 supplement (Invitrogen), the "AW-ITS" condition in which FBS was replaced by Insulin-Transferrin-Selenium supplement (ITS; Invitrogen) at concentrations of 0.1% from day 1 to day 2 and 1% from day 2 to day 7, and the "AS" condition in which WNT3A was removed from the growth factor combination.

4.5. Flow cytometry

Single cell suspensions were acquired through Accutase (Invitrogen) treatment. Cells were fixed and stained using the Transcription Factor Buffer Set (BD Biosciences) following the manufacturer's instructions. Conjugated antibodies were used, including T-PE, EOMES-APC, FOXA2-Alexa488, and SOX17-APC (all from R&D Systems; Table 1). Cells were resuspended in PBS supplemented with 1% BSA and analyzed using a BD Biosciences LSR II flow cytometry analyzer and BD FACSDiva software.

http://dx.doi.org/10.1016/j.heliyon.2015.e00046

Table 1. Antibody sources and dilutions.

Antibody	Source	Catalog Number	Dilution
OCT4	Santa Cruz	sc-9081	1:1,000 (WB)
SOX2	Millipore	AB5603	1:500 (WB)
α-TUBULIN	Abcam	ab11304	1:10,000 (WB)
GAPDH	GeneScript	A00192	1:10,000 (WB)
T	R&D systems	AF2085	1:500 (WB/IF)
EOMES	Abcam	ab23345	1:500 (WB/IF)
SOX17	R&D systems	AF1924	1:500 (WB/IF)
FOXA2	Millipore	07-633	1:500 (WB/IF)
CER1	Thermo-Pierce	MA5-15554	1:500 (WB)
AFP	DAKO	A0008	1:500 (WB)
SOX1	R&D systems	AF3369	1:500 (WB)
PAX6	Covance	PRB-278P	1:500 (WB)
T-PE	R&D Systems	IC2085P	1:20 (FACS)
EOMES-APC	R&D Systems	IC6166A	1:20 (FACS)
FOXA2-Alexa488	R&D Systems	IC2400G	1:40 (FACS)
SOX17-APC	R&D Systems	IC1924A	1:20 (FACS)
Goat IgG-PE isotype control	R&D Systems	IC108P	1:20 (FACS)
Goat IgG-APC isotype control	R&D Systems	IC108A	1:20 (FACS)
Mouse IgG_{2B}-APC isotype control	BioLegend	400319	1:20 (FACS)
Goat IgG-Alexa488 isotype control	R&D Systems	IC108G	1:40 (FACS)

4.6. KINOMEscan (DiscoveRx)

In this screen, DNA-tagged recombinant kinases were bound by ligands linked to a solid support. When a small molecule inhibitor was added, it will bind to its target kinase(s), either at the ligand-binding sites which directly competes with the ligand, or at other parts of the protein which indirectly inhibits ligand-binding of the kinase by inducing conformational changes. This inhibition will release the target kinase of this small molecule from its ligand, and kinases released from the solid support will be detected by PCR analysis through their DNA tags. Results for binding interactions were reported as Percent of Control (%Ctrl): %Ctrl = [(positive control signal – test compound signal)/(positive control signal – negative control signal)] × 100. DMSO was used as negative control. Lower values of % Ctrl indicate stronger interactions between the test compound and the kinases.

4.7. Western blotting

Cultured cells were lysed directly by 2× Laemmli buffer (Bio-Rad), boiled for 5 min, and analyzed using SDS-PAGE electrophoresis followed by wet-transfer

http://dx.doi.org/10.1016/j.heliyon.2015.e00046

onto nitrocellulose membranes using a system manufactured by Bio-Rad. The membranes were blocked using blocking solution (5% BSA in Tris-buffered saline containing 0.1% Tween-20 [TBST]), and then incubated with primary antibodies (Table 1), diluted in TBST, at 4 °C overnight. The membranes were then washed by TBST for 3 × 5 min, and incubated with horse radish peroxidase (HRP) conjugated secondary antibodies at room temperature for 1 hr. Finally, the membranes were washed 3–5 × 5 min by TBST and developed using Super-Signal West Pico Chemiluminescent Substrate (Pierce).

4.8. Neural differentiation

Neural differentiation were conducted as previously reported (Zhou et al., 2010). Briefly, hESCs were dissociated by Accutase (Invitrogen) and seeded onto culture plates pre-coated with Matrigel (BD Biosciences) in mTeSR1 medium (StemCell Technologies) supplemented with Y-27632 (10 μM; Calbiochem). Cultures were let grow till complete confluency and then changed into neural induction medium composed of Advanced DMEM/F12, 1% N-2 supplement, and Glutamax (all from Invitrogen) and supplemented with or without Dorsomorphin (1 μM; Sigma). Medium was changed every day. Cells were collected on day 8 for analysis.

4.9. Immunofluorescent staining

Cells were washed once with phosphate-buffered saline (PBS) and fixed by 4% paraformaldehyde (Santa Cruz) at room temperature for 20 min, permeabilized by 0.5% Triton X-100 (Sigma) in PBS (PBST) for 15 min, and then blocked with 5% donkey serum (Sigma) in 0.1% PBST at room temperature for 1 hr. The samples were incubated with primary antibodies (Table 1) in 0.1% PBST at 4 °C overnight, washed three times by PBS, and then incubated with fluorescent-labeled secondary antibodies in 0.1% PBST at room temperature for 2 hr. Finally, the cells were incubated with DAPI for 5 min, washed three times by PBS, and subjected to fluorescent microscopy analysis (Zeiss).

4.10. RNA extraction, reverse transcription, and quantitative-PCR

Total RNA were isolated using RNeasy mini kit (QIAGEN). cDNAs were synthesized from the purified RNAs using Reverse Transcription System (Promega). Quantitative-PCR was performed using QuantiTech SYBR Green PCR kit (QIAGEN). Signals were analyzed using the comparative C_T method, and ACTB gene was used as an internal control. Primer sequences are listed in Table 2.

http://dx.doi.org/10.1016/j.heliyon.2015.e00046

Table 2. qPCR primers.

Primer Name	Forward Primer (5′–3′)	Reverse Primer (5′–3′)
ACTB	agagctacgagctgcctgac	cgtggatgccacaggact
T (Brachyury)	gctgtgacaggtacccaacc	catgcaggtgagttgtcagaa
EOMES	gtggggaggtcgaggttc	tgttctggaggtccatggtag
MIXL1	ggcgtcagagtgggaaatcc	gcagttcacatctacctcaagag
EVX1	ttcacccgagagcagattg	ccggttctggaaccacac
TBX6	gaacggcagaaactgtaagagg	gtgtgtctccgctcccatag
HAND1	aaaggccctacttccagagc	tgcgctgttaatgctctcag
MEOX1	aaagtgtcccctgcattctg	cactccagggttccacatct
MESP1	ctgttggagacctggatgc	cgtcagttgtcccttgtcac
SOX17	acgccgagttgagcaaga	tctgcctcctccacgaag
FOXA2	tgggagcggtgaagatggaagggcac	tcatgccagcgcccacgtacgacgac
CER1	acagtgcccttcagccagact	acaactacttttttcacagccttcgt
GSC	gaggagaaagtggaggtctggtt	ctctgatgaggaccgcttctg
GATA4	ggaagcccaagaacctgaat	gttgctggagttgctggaa
GATA6	aatacttcccccacaacacaa	ctctcccgcaccagtcat
AFP	agcttggtggtggatgaaac	ccctcttcagcaaagcagac
SOX7	ctcagggcagggaggtct	gcactcggataaggagagtcc

For TRPM6 isoform detection, cDNAs extracted from undifferentiated hESCs were used as templates for PCR amplification of the isoforms followed by agarose gel electrophoresis. For the sequences of isoform-specific PCR primers see Chubanov et al. (Chubanov et al., 2004).

4.11. Fugene HD transfection

Fugene HD reagent was purchased from Promega. Transfections were conducted following manufacturer's instructions. Briefly, plasmid DNA (Sigma TRC shRNA vectors; Table 3) and Fugene HD transfection reagent were mixed at a 3:1 ratio in Opti-MEM medium (Invitrogen), incubated 15 min at room temperature, and applied to cells at day -1 or day 0 of the A-BVF or AWS differentiation protocols. ROCK inhibitor Y-27632 was added during transfection to boost transfection efficiency as previously reported (Yen et al., 2014).

4.12. Intracellular magnesium analysis

The cell permeant magnesium ion sensor Mag-fluo-4 was purchased from Invitrogen. 10 μM Mag-fluo-4 was loaded into cells for 30 min at room temperature in the dark, washed with PBS, and then analyzed using a BD Biosciences LSR II flow cytometry analyzer and BD FACSDiva software.

http://dx.doi.org/10.1016/j.heliyon.2015.e00046

Table 3. Names and sequences of shRNAs.

Target	shRNA	Sequence (5′–3′)
TRPM6	TRPM6-1	ccggcctggcataaagaatgtatatctcgagatatacattctttatgccaggttttt
	TRPM6-2	ccggccctctaatctaaagcgagttctcgagaactcgctttagattagagggttttt
	TRPM6-3	ccggccaaattctaatggagtgtatctcgagatacactccattagaatttggttttt
	TRPM6-4	ccgggctccctatctgataactcaactcgagttgagttatcagatagggagctttttt
NEK3	NEK3-1	ccgggcagtcccatagaacagaaatctcgagatttctgttctatgggactgctttttt
	NEK3-2	ccggccttattatgtgcctccagaactcgagttctggaggcacataataaggttttt
	NEK3-3	ccggcgaagcataacacaccaagaactcgagttcttggtgtgttatgcttcgttttt

4.13. Statistical analysis

Statistical analyses were performed using Microsoft Excel.

Declarations

Author contribution statement

Yijie Geng: Conceived and designed the experiments; Performed the experiments; Analyzed and interpreted the data; Wrote the paper.

Bradley Feng: Performed the experiments.

Funding statement

This work was supported by the National Institutes of Health (NIH) (GM083812), the Illinois Regenerative Medicine Institute (IDPH 2006-05516), National Science Foundation (NSF) CAREER award (0953267), and NSF Science and Technology Center Emergent Behaviors of Integrated Cellular Systems (EBICS) (CBET-0939511).

Competing interest statement

The authors declare no conflict of interest.

Additional information

No additional information is available for this paper.

Acknowledgments

We thank Dr. Linzhao Cheng and Dr. Prashant Mali for generously providing the MMW2 hiPSC line, and Dr. Vladimir Chubanov for valuable scientific discussion.

http://dx.doi.org/10.1016/j.heliyon.2015.e00046

References

Bernardo, A.S., Faial, T., Gardner, L., Niakan, K.K., Ortmann, D., Senner, C.E., Callery, E.M., Trotter, M.W., Hemberger, M., Smith, J.C., et al., 2011. BRACHYURY and CDX2 mediate BMP-induced differentiation of human and mouse pluripotent stem cells into embryonic and extraembryonic lineages. Cell. Stem Cell. 9, 144–155.

Borowiak, M., Maehr, R., Chen, S., Chen, A.E., Tang, W., Fox, J.L., Schreiber, S.L., Melton, D.A., 2009. Small molecules efficiently direct endodermal differentiation of mouse and human embryonic stem cells. Cell. Stem Cell. 4, 348–358.

Cai, J., Zhao, Y., Liu, Y.X., Ye, F., Song, Z.H., Qin, H., Meng, S., Chen, Y.Z., Zhou, R.D., Song, X.J., et al., 2007. Directed differentiation of human embryonic stem cells into functional hepatic cells. Hepatology 45, 1229–1239.

Choi, C.H., Jeong, J.S., Yoo, B.I., Jin, Y.X., Moon, D.C., Yoo, H.S., Oh, S., Hong, S.P., Lee, Y.M., 2007. Sphingosine 1-phosphate and sphingosine kinase activity during chicken embryonic development. Arch. Pharm. Res. 30, 502–506.

Chubanov, V., Gudermann, T., Schlingmann, K.P., 2005a. Essential role for TRPM6 in epithelial magnesium transport and body magnesium homeostasis. Pflug. Arch. Eur. J. Phys. 451, 228–234.

Chubanov, V., Schlingmann, K.P., Waring, J., Heinzinger, J., Kaske, S., Waidegger, S., Schnitzler, M.M.Y., Gudermann, T., 2007. Hypomagnesemia with secondary hypocalcemia due to a missense mutation in the putative pore-forming region of TRPM6. J. Biol. Chem. 282, 7656–7667.

Chubanov, V., Schlingmann, K.P., Waring, J., Schnitzler, M.M.Y., Waldegger, S., Gudermann, T., 2006. Dominant-negative effect of a novel missense mutation in the human TRPM6 gene associated with hypomagnesemia with secondary hypocalcemia. N-S. Arch. Pharmacol. 372, 60–61.

Chubanov, V., Schnitzler, M.M.Y., Waring, J., Plank, A., Gudermann, T., 2005b. Emerging roles of TRPM6/TRPM7 channel kinase signal transduction complexes. N-S. Arch. Pharmacol. 371, 334–341.

Chubanov, V., Waldegger, S., Schnitzler, M.M., Vitzthum, H., Sassen, M.C., Seyberth, H.W., Konrad, M., Gudermann, T., 2004. Disruption of TRPM6/TRPM7 complex formation by a mutation in the TRPM6 gene causes hypomagnesemia with secondary hypocalcemia. Proc. Natl. Acad. Sci. USA 101, 2894–2899.

Conlon, F.L., Lyons, K.M., Takaesu, N., Barth, K.S., Kispert, A., Herrmann, B., Robertson, E.J., 1994. A primary requirement for nodal in the formation and

http://dx.doi.org/10.1016/j.heliyon.2015.e00046

maintenance of the primitive streak in the mouse. Development 120, 1919–1928.

D'Amour, K.A., Agulnick, A.D., Eliazer, S., Kelly, O.G., Kroon, E., Baetge, E.E., 2005. Efficient differentiation of human embryonic stem cells to definitive endoderm. Nat. Biotechnol. 23, 1534–1541.

Evseenko, D., Zhu, Y., Schenke-Layland, K., Kuo, J., Latour, B., Ge, S., Scholes, J., Dravid, G., Li, X., MacLellan, W.R., et al., 2010. Mapping the first stages of mesoderm commitment during differentiation of human embryonic stem cells. Proc. Natl. Acad. Sci. USA 107 (31), 13742–13747.

Geng, Y., Zhao, Y., Schuster, L.C., Feng, B., Lynn, D.A., Austin, K.M., Stoklosa, J.D., Morrison, J.D., 2015. A Chemical Biology Study of Human Pluripotent Stem Cells Unveils HSPA8 as a Key Regulator of Pluripotency. Stem Cell Rep. In press.

Groenen, P.M., van Rooij, I.A., Peer, P.G., Ocke, M.C., Zielhuis, G.A., Steegers-Theunissen, R.P., 2004. Low maternal dietary intakes of iron, magnesium, and niacin are associated with spina bifida in the offspring. J. Nutr. 134, 1516–1522.

Huigens, R.W., Morrison, K.C., Hicklin, R.W., Flood, T.A., Richter, M.F., Hergenrother, P.J., 2013. A ring-distortion strategy to construct stereochemically complex and structurally diverse compounds from natural products. Nat. Chem. 5, 195–202.

Hurley, L.S., Cosens, G., Theriault, L.L., 1976. Teratogenic effects of magnesium deficiency in rats. J. Nutr. 106, 1254–1260.

Jin, J., Desai, B.N., Navarro, B., Donovan, A., Andrews, N.C., Clapham, D.E., 2008. Deletion of Trpm7 disrupts embryonic development and thymopoiesis without altering Mg(2+) homeostasis. Science 322, 756–760.

Jin, J., Wu, L.J., Jun, J., Cheng, X.P., Xu, H.X., Andrews, N.C., Clapham, D.E., 2012. The channel kinase, TRPM7, is required for early embryonic development. Proc. Natl. Acad. Sci. USA 109, E225–E233.

Komiya, Y., Su, L.T., Chen, H.C., Habas, R., Runnels, L.W., 2014. Magnesium and embryonic development. Magnes. Res. 27, 1–8.

Li, M., Jiang, J., Yue, L., 2006. Functional characterization of homo- and heteromeric channel kinases TRPM6 and TRPM7. J. Gen. Physiol. 127, 525–537.

Liu, P., Wakamiya, M., Shea, M.J., Albrecht, U., Behringer, R.R., Bradley, A., 1999. Requirement for Wnt3 in vertebrate axis formation. Nat. Genet. 22, 361–365.

 http://dx.doi.org/10.1016/j.heliyon.2015.e00046

Liu, W., Su, L.T., Khadka, D.K., Mezzacappa, C., Komiya, Y., Sato, A., Habas, R., Runnels, L.W., 2011. TRPM7 regulates gastrulation during vertebrate embryogenesis. Dev. Biol. 350, 348–357.

Ludwig, T.E., Levenstein, M.E., Jones, J.M., Berggren, W.T., Mitchen, E.R., Frane, J.L., Crandall, L.J., Daigh, C.A., Conard, K.R., Piekarczyk, M.S., et al., 2006. Derivation of human embryonic stem cells in defined conditions. Nat. Biotechnol. 24, 185–187.

Mali, P., Chou, B.K., Yen, J., Ye, Z., Zou, J., Dowey, S., Brodsky, R.A., Ohm, J.E., Yu, W., Baylin, S.B., et al., 2010. Butyrate greatly enhances derivation of human induced pluripotent stem cells by promoting epigenetic remodeling and the expression of pluripotency-associated genes. Stem Cells 28, 713–720.

Miller, J.C., Landesman, R., 1977. Magnesium deficiency in embryos of Xenopus laevis. J. Embryol. Exp. Morphol. 39, 97–113.

Nilius, B., Flockerzi, V., 2014. Mammalian transient receptor potential (TRP) cation channels. Preface. Handb. Exp. Pharmacol. 223, v–vi.

Norrman, K., Strombeck, A., Semb, H., Stahlberg, A., 2013. Distinct gene expression signatures in human embryonic stem cells differentiated towards definitive endoderm at single-cell level. Methods 59, 59–70.

Oh, S., Lee, D., Kim, T., Kim, T.S., Oh, H.J., Hwang, C.Y., Kong, Y.Y., Kwon Lim, K.S.D.S., 2009. Crucial role for Mst1 and Mst2 kinases in early embryonic development of the mouse. Mol. Cell. Biol. 29, 6309–6320.

Schlingmann, K.P., Waldegger, S., Konrad, M., Chubanov, V., Gudermann, T., 2007. TRPM6 and TRPM7 - Gatekeepers of human magnesium metabolism. Bba-Mol. Basis. Dis. 1772, 813–821.

Thomson, J.A., Itskovitz-Eldor, J., Shapiro, S.S., Waknitz, M.A., Swiergiel, J.J., Marshall, V.S., Jones, J.M., 1998. Embryonic stem cell lines derived from human blastocysts. Science 1145–1147.

Tian, Y., Lei, L., Cammarano Nekrasova, M.T., Minden, A., 2009. Essential role for the Pak4 protein kinase in extraembryonic tissue development and vessel formation. Mech. Dev. 126, 710–720.

Walder, R.Y., Yang, B.L., Stokes, J.B., Kirby, P.A., Cao, X., Shi, P.J., Searby, C.C., Husted, R.F., Sheffield, VC, 2009. Mice defective in Trpm6 show embryonic mortality and neural tube defects. Hum. Mol. Genet. 18, 4367–4375.

Wang, F.L., Wang, R., Khairallah, E.A., Schwartz, R., 1971. Magnesium depletion during gestation and lactation in rats. J. Nutr. 101, 1201–1209.

 http://dx.doi.org/10.1016/j.heliyon.2015.e00046

Yen, J., Yin, L., Cheng, J., 2014. Enhanced Non-Viral Gene Delivery to Human Embryonic Stem Cells via Small Molecule-Mediated Transient Alteration of Cell Structure. J. Mater. Chem. B. Mater. Biol. Med. 2, 8098–8105.

Yu, P., Pan, G., Yu, J., Thomson, J.A., 2011. FGF2 sustains NANOG and switches the outcome of BMP4-induced human embryonic stem cell differentiation. Cell. Stem. Cell. 8, 326–334.

Zhou, J., Su, P., Li, D., Tsang, S., Duan, E., Wang, F., 2010. High-efficiency induction of neural conversion in human ESCs and human induced pluripotent stem cells with a single chemical inhibitor of transforming growth factor beta superfamily receptors. Stem Cells 28, 1741–1750.